Oligocene–Miocene paleoceanography off the Wilkes Land margin (East Antarctica) based on organic-walled dinoflagellate cysts

Peter K. Bijl[1]*, Alexander J. P. Houben[2], Julian D. Hartman[1], Jörg Pross[3], Ariadna Salabarnada[4], Carlota Escutia[4], Francesca Sangiorgi[1]

1 Marine Palynology and Paleoceanography, Laboratory of Palaeobotany and Palynology, Department of Earth Sciences, Faculty of Geosciences, Utrecht University. P.O. Box 80.115, 3508 TC Utrecht, The Netherlands

2 Geological Survey of the Netherlands, Netherlands Organisation for Applied Scientific Research (TNO), Princetonlaan 6, 3584 CB, Utrecht, The Netherlands

3 Paleoenvironmental Dynamics Group, Institute of Earth Sciences, Heidelberg University, Im Neuenheimer Feld 234, 69120 Heidelberg, Germany

4 Instituto Andaluz de Ciencias de la Tierra, CSIC-UGR, 18100 Armilla, Spain

* to whom correspondence should be addressed.
Email: p.k.bijl@uu.nl; phone +31 30 253 9318

Abstract

Next to atmospheric CO_2 concentrations, ice-proximal oceanographic conditions are a critical factor for the stability of Antarctic marine-terminating ice sheets. The Oligocene and Miocene epochs (~34–5 Ma ago) were time intervals with atmospheric CO_2 concentrations between those of present-day and those expected for the near future. As such, these past analogues may provide insights into ice-sheet volume stability under warmer-than-present-day climates. We present organic-walled dinoflagellate cyst (dinocyst) assemblages from chronostratigraphically well-constrained Oligocene to mid-Miocene sediments from Integrated Ocean Drilling Program Expedition (IODP) Site U1356. Situated offshore the Wilkes Land continental margin, East Antarctica, the sediments from Site U1356 have archived the dynamics of an ice sheet that is today mostly grounded below sea level. We interpret dinocyst assemblages in terms of paleoceanographic change on different time scales, i.e., with regard to both glacial-interglacial and long-term variability. Our record shows that a sea-ice related dinocyst species, *Selenopemphix antarctica*, occurs only for the first 1.5 Ma of the early Oligocene, following the onset of full continental glaciation on Antarctica, and after the mid-Miocene Climatic Optimum. Dinocysts suggest a weaker-than-modern sea-ice season for the remainder of the Oligocene and Miocene. The assemblages generally bear strong similarity to present-day open-ocean, high-nutrient settings north of the sea-ice edge, with episodic dominance of temperate species similar to those found in the present-day subtropical front. Oligotrophic and temperate surface waters prevailed over the site notably during interglacial times, suggesting that

the positions of the (subpolar) oceanic frontal systems have varied in concordance with Oligocene-Miocene glacial-interglacial climate variability.

1. Introduction

The proportion of the East Antarctic ice sheet that is presently grounded below sea level is much larger than originally interpreted (Fretwell et al., 2013). This implies that a larger part of the continental ice sheet is sensitive to basal melting by warm waters than previously thought (Shepherd et al., 2012; Rignot et al., 2013; Wouters et al., 2015), and that a higher amplitude and faster rate of sea-level rise is to be expected under future climate warming than previously acknowledged (IPCC, 2013). Studying the amount and variability of Antarctic ice volume in periods with high atmospheric CO_2 concentrations (pCO_2) provides additional insight into ice/ocean feedback processes. Foster and Rohling (2013) compared sea-level and atmospheric pCO_2 concentrations on geological timescales. Their study suggests that global ice sheets were rather insensitive to climate change when atmospheric pCO_2 ranged between 400 and 650 parts per million in volume (ppmv). During the Oligocene and Miocene, atmospheric pCO_2 ranged between 400 and 650 ppmv (Foster et al., 2012; Badger et al., 2013; Greenop et al., 2014). Crucially, similar pCO_2 levels are expected for the near future given unabated carbon emissions (IPCC, 2013), implying that global ice volume may not change much under these pCO_2 scenarios.

In contrast to the invariant global ice volume inferred by Foster and Rohling (2013), a strong (up to 1 per mille; ‰) variability is preserved in deep-sea benthic foraminiferal oxygen isotope (hereafter benthic $\delta^{18}O$) data (e.g., Pälike et al., 2006a; Beddow et al., 2016; Holbourn et al., 2007; Liebrand et al., 2011; 2017; De

Vleeschouwer et al., 2017). These benthic $\delta^{18}O$ data reflect changes in continental ice volume (primarily on Antarctica) and deep-sea temperature. The latter is strongly coupled to polar surface-water temperature, as deep-water formation was predominantly at high latitudes at that time (Herold et al., 2011). High-amplitude variations in benthic $\delta^{18}O$ thus suggest either (i) strong climate dynamics in the high latitudes with relatively minor ice-volume change (which would be in accordance with numerical modelling experiments (Barker et al., 1999) and the interpretation of Foster and Rohling (2013)), or (ii) strong fluctuations in Antarctic ice volume, with relatively subdued temperature variability (which would be in accordance with indications for unstable Antarctic ice sheets under warmer-than-present climates (Cook et al., 2013; Greenop et al., 2014; Rovere et al., 2014; Sangiorgi et al., 2018). If one assumes a present-day $\delta^{18}O$ composition (-42‰ *versus* standard mean ocean water (SMOW)) for Oligocene–Miocene Antarctic ice-sheets and modern deep-water temperature (2.5°C), the benthic $\delta^{18}O$ fluctuations during the Oligocene–Miocene suggest long-term ice-sheet variability to have fluctuated considerably (Liebrand et al., 2017). Similarly strong fluctuations were observed in sedimentary records from the Gippsland Basin, southeast Australia (Gallagher et al., 2013). Meanwhile, deep-sea temperatures have fluctuated considerably as well during the Oligocene and Miocene (Lear et al., 2004), which is further evident from ice-free geologic episodes (Zachos et al., 2008). Therefore, a combination of deep-sea temperature and ice-volume changes is likely represented in these records. Further ice-proximal reconstructions of climate, ice-sheet and oceanographic conditions are required to provide an independent assessment of the stability of ice sheets under these higher-than present-day pCO_2 concentrations.

While Oligocene–Miocene climates may bear analogy to our future in terms of pCO_2 concentrations, the uncertainties and differences in Antarctic paleotopography must be considered in any such comparison, as this factor critically determines the proportion of marine-based *versus* land-based ice. An Antarctic continent with low topography would result in more ice sheets being potentially sensitive to basal melt and as such a higher sensitivity of these ice sheets to climate change. Moreover, the fundamentally different paleogeographic configuration of the Southern Ocean during that time as compared to today should also be considered (Figure 1). The development and strength of the Antarctic Circumpolar Current (ACC) connecting the Atlantic, Indian and Pacific Ocean basins (Barker and Thomas, 2004; Olbers et al., 2004) depend on the basin configuration (i.e., the width and depth of the gateways as well as the position of the landmasses). The exact timing when the ACC reached its modern-day strength is still uncertain, ranging from the middle Eocene (41 Ma) to as young as Miocene (23 Ma; Scher and Martin, 2004; Hill et al., 2013; Scher et al., 2015). Whether and, if so, how the development of the ACC has influenced latitudinal heat transport, ice-ocean interactions and the stability of Antarctic continental ice has remained poorly understood.

To directly assess the role of ice-proximal oceanography on ice-sheet stability during the Oligocene–Miocene, ice-proximal proxy-records are required. Several ocean drilling expeditions have been undertaken in the past to provide insight in the history of the Antarctic ice sheets (Barrett, 1989; Wise and Schlich, 1992; Barker et al., 1998; Robert et al., 1998; Wilson et al., 2000; Cooper and O'Brien, 2004; Exon et al., 2004; Harwood et al., 2006; Escutia and Brinkhuis, 2014). For some of the retrieved sedimentary archives, age control was particularly challenging due to the

paucity of useful means to calibrate them to the international time scale. As a consequence, the full use of these archives for the generation of paleoceanographic proxy records and ice-sheet reconstructions has remained limited.

In 2010, Integrated Ocean Drilling Program (IODP) Expedition 318 drilled an inshore-to-offshore transect off Wilkes Land (Fig. 1a), a sector of East Antarctica that is interpreted to be highly sensitive to continental ice-sheet melt (Escutia et al., 2011). The sediments recovered from IODP Site U1356 are from the continental rise of this margin (Escutia et al., 2011) and hence contain a mixture of shelf-derived material and pelagic sedimentation. Dinocyst events in this record have been recently tied to the international time scale through integration with calcareous nannofossil, diatom and magnetostratigraphic data (Bijl et al., 2018). By Southern Ocean standards, the resulting stratigraphic age frame for the Oligocene–Miocene record of Site U1356 (Fig. 2; Table 1) is of high resolution. In this paper, we investigate the dinocyst assemblages from this succession by utilizing the strong relationships between dinocyst assemblage composition and surface-water conditions of today's Southern Ocean (Prebble et al., 2013). We reconstruct the oceanographic regimes during the Oligocene and mid-Miocene, and evaluate their implications. We further compare the palynological data with lithological observations and their interpretations from Salabarnada et al. (submitted, this volume). Pairing the sedimentological interpretations and biomarker-derived absolute sea-surface temperature (SST) reconstructions from Site U1356 (Hartman et al., submitted, this volume) with our dinocyst assemblage data, we reconstruct the paleooceanographic conditions off Wilkes Land and assess their variability both on glacial-interglacial and longer-term times scales.

2. Material

2.1 Site description for IODP Hole U1356A

Samples were taken from IODP Hole U1356A, the only hole from Site U1356, cored on the continental rise of the Wilkes Land margin, East Antarctica (Figure 1a; present coordinates 63°18.6' S, 135°59.9' E; Escutia et al., 2011). The paleolatitude calculator of van Hinsbergen et al. (2015) was used to reconstruct the paleolatitudinal history of the site (Figure 1, between -59.8±4.8°S and -61.5±3.3° S between 34 Ma and 13 Ma, respectively). Hole U1356A reaches a depth of 1006.4 m into the seabed (Escutia et al., 2011). Oligocene to upper Miocene sediments were recovered between 890 and 3 mbsf (meters below sea floor, Figure 2; Tauxe et al., 2012; revised according to Bijl et al., 2018). The uppermost 95 meters of the hole were poorly recovered; sediments consisted of unconsolidated mud strongly disturbed by rotary drilling (Escutia et al., 2011). Hence, we focused our investigation on the interval between Cores 11R to 95R Section 3 (95.4–894 mbsf; 10.8–33.6 Ma; Figure 2).

2.2 Lithology in IODP Hole U1356A

In the interval between 95.4 and 894 mbsf, nine lithologic units have been recognized during shipboard analysis (Figure 2; Escutia et al., 2011). Salabarnada et al. (submitted, this volume) present a detailed lithologic column of the Oligocene and Miocene sediments. The lithologic facies described in Salabarnada et al. (submitted, this volume) will help us compare paleoceanographic differences between climatic extremes. Salabarnada et al. (submitted this volume) distinguished various lithologies along with interpretations of their depositional settings which can be summarized as:

1) laminated silty clay sediments (interpreted as glacial deposits; hereafter Fg), 2) bioturbated siltstones and claystones that in some intervals are carbonate-cemented (interpreted as interglacial deposits, hereafter Fi), and 3) perturbed mass transport deposits (MTDs): slumps and debris flows. We refer to Salabarnada et al. (submitted this volume; Fig S2) for a detailed description of these facies, and to the supplementary datasets on pangaea for more detailed separation of our palynological results per facies type.

2.3 Bio-magnetostratigraphic age model for IODP Hole U1356A

Stratigraphic constraints for the Oligocene–Miocene succession from IODP Hole U1356A are provided through calcareous nannoplankton, radiolarian, diatom and sparse palynological biostratigraphy, complemented by magnetostratigraphy (Tauxe et al., 2012). Bijl et al. (2018) and Crampton et al. (2016) have updated the existing age model for Site U1356 for the Oligocene and Miocene parts of the succession, respectively. In their efforts, they recalibrated the tie points to the international time scale of Gradstein et al. (2012). We here follow their revision of the age model (Table 1). We infer ages by linear interpolation between tie points (Figure 2; Table 1).

2.4 Depositional setting at IODP Site U1356

The depositional setting at Site U1356 changed from a shallow mid-continental shelf in the early Eocene (Bijl et al., 2013a) to a deep continental rise environment by the Oligocene (Houben et al., 2013) due to subsidence of the Wilkes Land margin (e.g., Close et al., 2009). Regional correlation of the facies at Hole U1356A via seismic profiles suggests a mix of distal-submarine fan and hemipelagic sedimentation during

the early Oligocene, grading into channel-levee deposits in the later Oligocene (Escutia et al., 2011). The boundary between these two different depositional settings is at ~650 mbsf; there, sedimentation rates increase, and the documentation of mass-transport deposits from this depth upwards suggests shelf-derived erosion events on the Wilkes Land continental slope (Escutia et al., 2011).

3. Methods

3.1 Palynological sample processing

The sample processing and analytical protocols as followed in this study are in accordance with standard procedures and have been previously described by Bijl et al. (2013b; 2018). The 25 species of dinocysts new to science, which are formally (2 species) and informally (23 species) described in Bijl et al. (2018), fit into known and extant genera, and therefore could be confidently included in the ecological groups as described below. We refer to Bijl et al. (2018) for an extensive overview (including plates) of the dinocyst species encountered.

3.2 Ecological grouping of dinocyst taxa

Bijl et al. (2018) provided additional statistical evidence to distinguish in situ dinocysts from those that are reworked from older strata. In this paper, we follow the interpretations of Bijl et al. (2018) and divide the dinocyst species into a reworked and an in situ group (Table 2). To use the in situ dinocyst assemblages for oceanographic reconstructions, we rely on the observation that many taxa in the fossil assemblages have morphologically closely related modern counterparts. This approach takes advantage of studies on the present-day relationship between

214 Southern Ocean microplankton in general and dinoflagellate cysts in particular and
215 their surface-water characteristics (e.g., Eynaud et al., 1999; Esper and Zonneveld,
216 2002, 2007; Prebble et al., 2013). We assign Oligocene–Miocene dinocyst taxa to
217 present-day eco-groups interpreted from the clusters identified by Prebble et al.
218 (2013), which appear to be closely related to the oceanic frontal systems in the
219 Southern Ocean (Figure 3). Supporting evidence for the ecologic affinities of the
220 dinocyst groups comes from empirical data, such as correlation of abundances with
221 other sediment properties or proxies (Sluijs et al., 2005; Egger et al., 2018), for
222 instance with regard to the affinities of *Nematosphaeropsis labyrinthus*,
223 *Operculodinium* spp., *Pyxidinopsis* cpx. (this includes *Corrudinium* spp. and
224 *Cerebrocysta* spp.) and *Impagidinium* spp. There is further abundant evidence, both
225 empirically (e.g., Sluijs et al., 2003; Houben et al., 2013) and from modern
226 observations (Zonneveld et al., 2013; Prebble et al., 2013; Eynaud et al., 1999), that
227 links the abundance of protoperidinioid dinocysts to high surface-water productivity.
228 The arguably most important inference from the surface-sediment sample study of
229 Prebble et al. (2013) is that *Selenopemphix antarctica* is common to dominant (10–
230 90%) south of the Antarctic polar front (AAPF). In particular, the Antarctic
231 continental shelf exhibits a consistently high relative abundance of *Selenopemphix*
232 *antarctica*. In addition to the surface samples of Prebble et al. (2013), this is also
233 evident at the Wilkes Land margin proper (IODP Site U1357; Hartman, Bijl and
234 Sangiorgi, pers. obs.), at Prydz Bay (Storkey, 2006), in the Weddell (Harland and
235 Pudsey, 1999) and Ross Seas (Hartman, Bijl and Sangiorgi, pers. obs), and in the
236 southern Indian Ocean (Marret and de Vernal, 1997): samples all contain very
237 abundant to dominant (>50 to 90%) *S. antarctica*. The dominance of this species

becomes even stronger when considering that assemblages in these surface samples often include cysts that are not easily preserved in older sediments such as that of *Polarella glacialis*. Leaving these dinocyst out of the dinocyst sum increases the relative abundance of *Selenopemphix antarctica* in surface samples. Notably, surface-sediment samples outside of the AAPF never have dominant (~90%) *Selenopemphix antarctica* (Prebble et al., 2013). Another important observation is that the surface-sediment samples south of the AAPF are generally devoid of gonyaulacean dinocysts, with the exception of two species of *Impagidinium* (i.e., *I. pallidum* and *I. sphaericum*) that may occur, although neither abundantly (Prebble et al., 2013) nor exclusively (e.g., Zevenboom, 1995; Zonneveld et al., 2013), in ice-proximal locations. Abundant *Nematosphaeropsis labyrinthus* occurs exclusively in regions outside of the Subantarctic Front, and particularly near the Subtropical Front. Thus, we conclude from the available literature a dominance of *S. antarctica* south of the AAPF, a dominance of other protoperidinioid dinocysts at and north of the AAPF, mixed protoperidinioid and gonyaulacoid dinocysts (with a notable occurrence of *Nematosphaeropsis labyrinthus* at the sub-Antarctic front (SAF), and mixed gonyaulacoid dinocysts at and outside of the subtropical front (STF). These trends represent a north-south transition from sea-ice-influenced to cold upwelling/high nutrient to warm-temperate/lower nutrient conditions, respectively. We use these affinities to reconstruct past oceanographic conditions at the Wilkes Land continental margin.

4. Results

4.1 Palynological groups

In our palynological analysis we separated palynomorph groups into four categories: reworked dinocysts (following Bijl et al. (2018); Table 2), in situ dinocysts, acritarchs, and terrestrial palynomorphs. Our palynological slides further contain a varying amount of pyritized diatoms and a minor component of amorphous organic matter, which is not further considered in this study. The relative and absolute abundances of the four palynomorph groups vary considerably throughout the studied interval (Figure 4). Reworked dinocysts are ubiquitous throughout the record, and are particularly abundant in the lowermost 40 meters of the Oligocene and in the Upper Oligocene. In situ dinocysts dominate mid-Oligocene and mid-Miocene palynomorph assemblages. Chorate, sphaeromorph and *Cymatiosphaera*-like acritarchs (which are not further taxonomically subdivided) dominate the assemblage in the Upper Oligocene and into the mid-Miocene, while terrestrial palynomorphs (which are considered in situ and not reworked from older strata (Strother et al., 2017)) are a constant minor (a few % of the total palynomorph assemblage) component of the total palynomorph assemblage (Fig. 4). The terrestrial palynomorphs and the paleoclimatic and paleoecological interpretations derived from them will be presented in another study.

4.2 In situ dinocyst assemblages

Throughout the Oligocene, in situ dinocyst assemblages are dominated by protoperidinioid dinocysts, notably *Brigantedinium* spp., *Lejeunecysta* spp., *Malvinia escutiana,* and *Selenopemphix* spp. (Figure 4), all of which are cysts of heterotrophic dinoflagellates (e.g., Esper and Zonneveld, 2007). Among these protoperidinioid cysts, *S. antarctica* is frequently present (up to 39% of the in situ assemblage), but

only between 33.6 and 32.1 Ma (earliest Oligocene) and after 14.2 Ma (i.e., during and after the mid-Miocene climatic transition; Fig. 5). The remainder of the record is almost entirely devoid of *S. antarctica*. This is much in contrast to the dinocyst assemblages nearby Site U1356 today, which are dominated by this taxon (Prebble et al., 2013). Instead of *S. antarctica*, other protoperidinioid dinocysts dominate during the Oligocene and Miocene, such as *Brigantedinium* spp., several *Lejeunecysta* species and *Selenopemphix nephroides*, which have close affinities to high-nutrient conditions in general (e.g., Harland et al., 1999; Zonneveld et al., 2013), but are not specifically restricted to sea-ice-proximity or the Southern Ocean. Today, these three genera dominate dinocyst assemblages in high-nutrient settings at or outside of the AAPF (Prebble et al., 2013). A varying abundance of protoperidinioid dinocysts could not be placed with confidence into established protoperidinioid dinocyst genera. These are grouped under 'protoperidinioid spp. pars' (Figure 4; Bijl et al., 2018) and are here assumed to exhibit the same heterotrophic life-style as the other protoperidinioid dinocyst genera.

Next to protoperidinioid dinocysts, gonyaulacoid dinocysts also occur in relatively high abundances throughout the record from Site U1356. They comprise both known and previously unknown (Bijl et al., 2018) species of *Batiacashaera, Pyxidinopsis, Corrudinium, Cerebrocysta, Nematosphaeropsis, Impagidinium, Operculodinium*, and *Spiniferites* (Fig. 4; 5). The 'others' group represents exclusively gonyaulacoid species such as *Invertocysta tabulata* and *Gelatia inflata*. Except for the extinct genera *Batiacasphaera* and *Cerebrocysta* and some genera in the 'others' group, all the other genera are still extant and represent phototrophic dinoflagellates (Zonneveld et al., 2013). Their abundance is at the expense of the assumed heterotrophic

310 protoperidinioid dinocysts. A marked increase in abundance of gonyaulacoid cysts is
311 associated with the mid-Miocene Climate Optimum (MMCO between ~17 and 15 Ma;
312 Fig. 4, 5; Sangiorgi et al., 2018). Of the gonyaulacoid taxa, *Nematosphaeropsis*
313 *labyrinthus* is associated with frontal systems of the present-day Southern Ocean
314 (Prebble et al., 2013) and of the North Atlantic Ocean (Boessenkool et al., 2001;
315 Zonneveld et al., 2013).
316
317 4.3 Comparison between palynological data and lithological facies
318 The Oligocene-Miocene sediments from Site U1356 comprise distinctive alternations
319 of lithologic facies throughout the section (Salabarnada et al., submitted, this volume;
320 Figure S2). Laminated (Fg) and bioturbated sediments, that are in some intervals are
321 carbonate-rich (Fi) alternate on orbital time scales and this pattern is in some
322 intervals disrupted by slumps and/or debris flows. We here evaluate and compare
323 the palynological content of each of these facies both in terms of absolute and relative
324 abundance of the main palynomorph groups: reworked dinocysts, in situ dinocysts,
325 acritarchs and terrestrial palynomorphs, and relative abundance of in situ dinocyst
326 eco-groups.
327
328 4.3.1 Palynomorph groups and lithology
329 There are distinct differences in the relative and absolute abundances of the
330 palynomorph groups between the different lithologies (Figure 6). The highest relative
331 and absolute abundances of reworked dinocysts occur in the slump and Fi facies (Fig.
332 6), particularly those of early Oligocene age (EOT slumps and bioturbated siltstones
333 in Supplementary datasets), in line with observations of Houben et al. (2013).

Reworking is a minor component of the palynomorph assemblage in the other lithologies for most samples, with a higher absolute abundance in Fi deposits than in glacial deposits. This suggests that submarine erosion of Eocene continental shelf material was particularly prominent during interglacial times, when arguably sea level along the Wilkes Land margin was lower (Stocchi et al., 2013). The relative and absolute abundance of *in-situ* dinocysts is highest in the interglacial and glacial deposits and the slumps (Figure 6). Acritarchs reach highest relative and absolute abundances in Fi facies and in the debris flows (Figure 6). Terrestrial palynomorphs are most abundant in the lower Oligocene slumps and Fi sediments (Supplementary tables) but have low relative abundance in all lithologies (Figure 6).

4.3.2 In situ dinocyst eco-groups and their abundance per facies

The in situ dinocyst eco-groups are also compared with the lithological facies (Figure 7). The Fg glacial facies contains generally more peridinioid (heterotrophic) dinocysts, while the Fi interglacial facies contains more gonyaulacoid (oligotrophic) dinocysts, but more information is to be seen when focussing on the individual eco-groups. The abundance of *Selenopemphix antarctica* is low throughout the record (0–5%), with the exception of the interval post-dating the MMCO and the lowermost Oligocene, where the taxon reaches occasionally more than 20% (Figs. 4, 5). *S. antarctica* reaches highest abundances in the slump facies and Fg and is less abundant in the other lithologies (Figure 7). *Selenopemphix* spp. reaches highest relative abundances in the Fg facies. *Lejeunecysta* spp. and *Protoperidinium* spp. pars. show no noticeable variance in relative abundance in any of the lithologies. *Brigantedinium* spp. is clearly higher abundant in the Fg facies than in the Fi facies.

358 *Malvinia escutiana* abundances seem to be higher in Fi than in Fg (Figure 7), although
359 this species has a stratigraphic occurrence that is limited to the early Oligocene (Bijl
360 et al., 2018). *Nematosphaeropsis labyrinthus*, *Pyxidinopsis* cpx, *Operculodinium* spp.,
361 and *Impagidinium* spp. reach higher relative abundances in Fi than in Fg facies,
362 whereas the abundance of *Batiacasphaera* spp. seems invariant to facies.
363
364 **5. Discussion**
365 5.1 Paleoceanographic interpretation of the dinocyst assemblages
366 The composition of the dinoflagellate cyst assemblages in the Wilkes Land record
367 reflect changes in surface-ocean nutrients, sea- surface temperature conditions and
368 paleoceanographic features. We will discuss these implications in the following.
369
370 5.1.1 Surface-ocean nutrient conditions
371 The general dominance of heterotrophic dinocysts in the Oligocene–Miocene
372 assemblages indicates overall high nutrient levels in the surface waters. Given the
373 offshore geographic setting, we therefore infer that surface waters at Site U1356
374 experienced upwelling associated to the AAPF during most of the Oligocene and
375 Miocene. We can exclude the possibility that nutrients were brought to the site via
376 river runoff given the anticipated small catchment area that experienced liquid
377 precipitation in the Wilkes Land hinterland, the low amounts of terrestrially-derived
378 (amorphous) organic matter in the palynological residues and relatively low
379 branched over isoprenoid tetraether (BIT) index values (Hartman et al., submitted
380 this volume) that indicates predominantly marine organic matter. The exception may

be the mid-Miocene climatic Optimum (Sangiorgi et al., 2018) when considerable soil-derived organic matter reached the site.

The occasionally abundant gonyaulacoid cyst taxa encountered in our record suggest that at times surface waters were much less nutrient-rich supported the growth of oligotrophic dinoflagellates. Notably, these taxa are typical for outer-shelf to oceanic or outer neritic settings (e.g., Sluijs et al., 2005; Zonneveld et al., 2013; Prebble et al., 2013), which makes it unlikely that they were reworked from the continental shelf. Indeed, they show low relative abundances in the perturbed deposits (Figure 7). Although the members of these genera have relatively long stratigraphic ranges extending back into the Eocene, most of the species encountered at Site U1356 are not present in Eocene continental shelf sediments in the region (e.g., Wrenn and Hart, 1988; Levy and Harwood, 2000; Brinkhuis et al., 2003a, b; Bijl et al., 2011; 2013a, b). This makes it unlikely that they are reworked from Eocene strata. In addition, statistical analysis also yields that these species are part of the in situ assemblage (Bijl et al., 2018). These different lines of evidence lead us to interpret them as part of the in situ pelagic assemblage in our study, which allows us to interpret their paleoceanographic implications based on their modern affinities. The absence of these taxa in modern surface waters south of the AAPF is probably caused by a combination of different factors: It can be connected to low sea-surface temperatures and an isolation by strong eastward currents, but also the abundance and seasonally concentrated availability of nutrients, all of which make the proximal surface waters off Antarctica a highly specialistic niche unfavourable for these species. Apparently, surface-water conditions during the Oligocene and Miocene were

such that these oligotrophic species could at times proliferate so close to the Antarctic margin.

5.1.2 Sea-surface temperature

The best modern analogues for the dinocyst assemblages in our record are to be sought off the southern margins of New Zealand and Tasmania (as inferred from Prebble et al., 2013; Figure 2). Today, these regions feature a mix between protoperidinioid dinocysts along with gonyaulacoid dinocyst genera such as *Nematosphaeropsis*, *Operculodinium* and *Impagidinium*. These assemblages prevail in surface waters with mean annual temperatures of 8–17°C (Prebble et al., 2013) and therefore suggest relatively warm surface water temperatures close to the Wilkes Land margin. In support of this, a bayesian approach on the TEX_{86} index values at Site U1356 (presented in Sangiorgi et al., 2018; Hartman et al., submitted, this volume) also suggests the Southern Ocean mid-latitudes as a modern-analogue region and reconstructs a paleotemperature range of 8–20°C for the Oligocene–Miocene at Site U1356, with values in excess of 24°C for the late Oligocene (Hartman et al., submitted, this volume). Futher, supporting evidence for temperate Oligocene–Miocene surface waters comes from the abundance of nannofossils encountered in the sediments (Escutia et al., 2011; Salabarnada et al., submitted this volume). Today, carbonate-producing plankton is rare in high-latitude surface waters south of the AAPF (Eynaud et al., 1999). Moreover, the remains of the few pelagic carbonate-producing organisms living at high latitudes rarely reach the ocean floor because of strong upwelling of relatively CO_2-rich, corrosive waters (e.g., Olbers et al., 2004). Hence, the presence of carbonate-rich intervals during the Oligocene–Miocene at Site U1356

along with the encountered oligotrophic, temperate dinocysts suggests fundamentally warmer surface-water conditions than today.

5.1.3 Surface paleoceanography

The strong similarity of Oligocene–Miocene dinocyst assemblages at Site U1356 with those today occurring much further north (i.e.., around Tasmania and Southern New Zealand (Prebble et al., 2013) suggests a fundamentally different *modus operandi* of Southern Ocean surface oceanography. The strict latitudinal separation of dinocyst assemblages in the Southern Ocean today (Prebble et al., 2013) is likely due to different surface water masses present across the oceanic fronts where strong wind-driven divergence around 60° S (known as the Antarctic Divergence; e.g., Olbers et al., 2004), strong sea-ice season and/or the vigorous Antarctic Circumpolar Current are in place. The strength and position of the AAPF during the Oligocene–Miocene is not well understood. Climate model (GCM) experiments under Miocene boundary conditions suggest that west and east wind drifts prevailed south and north of 60°S, respectively (Herold et al., 2011). This wind orientation determined the average position of the Antarctic Divergence at 60°S during the Oligocene and Miocene, similar to today. This suggests that Site U1356 was likely directly overlain by the AAPF. However, the significantly warmer, more oligotrophic dinocyst assemblages off Wilkes Land throughout the Oligocene–Miocene argue against proximity to the AAPF. The position of the AAPF relative to that of Site U1356 strongly determines the likelihood of southward transport of low-latitude waters towards the site. A southward position of the AAPF relative to Site U1356 would greatly enhance the possibility for a southward migration of temperate surface water masses towards the

site. A northward position of the AAPF relative to the site would make such a latitudinal migration much more difficult. The presence of carbonate in these deep marine sediments also suggests that upwelling of corrosive waters through the (proto-)Antarctic Divergence was either much reduced or located elsewhere. Therefore, we deduce that the occurrence of the oligotrophic, temperate dinocysts is an evidence for a southward position of the AAPF relative to the position of Site U1356. This would allow a higher connectivity between the site and the lower latitudes, and promote preservation of carbonate on the sea floor. Also, such an oceanographic setting would be in line with reduced sea ice along the Wilkes Land margin.

The separate averaging of dinocyst assemblages for glacial and interglacial facies from Site U1356 (Figure 7) allows us to reconstruct glacial-interglacial changes in surface-water conditions throughout the Oligocene. First of all, our observations suggest that Oligocene glacial-interglacial cycles were connected to substantial paleoceanographic dynamics off Wilkes Land. In agreement with the 2–3 °C SST variability as documented for this site during glacial-interglacial cycles (Hartman et al., submitted, this volume), dinocyst assemblages contain more oligotrophic, temperate dinocysts during interglacial times compared to glacial times when more eutrophic, colder dinocysts proliferated (Fig. 7). This could be the result of a slight latitudinal movement of oceanic frontal systems (notably the AAPF) as it has been reconstructed for the Southern Ocean fronts during the most recent glacial to interglacial transition (e.g., Bard and Rickaby, 2009; Kohfeld, et al., 2013; Xiao et al., 2016). In such a scenario, the AAPF would reach a southern position during interglacials, allowing for temperate oligotrophic surface waters to reach the site,

476 while it would migrate northward over Site U1356 during glacials, thereby causing
477 cold, high-nutrient surface-water conditions and obstructing low-latitude influence.
478
479 5.2 Implications for Oligocene–Miocene ocean circulation
480 At Site U1356, dinocyst assemblages bear similarities to present-day proximal-
481 Antarctic assemblages (Prebble et al., 2013) only in the lowermost Oligocene and in
482 strata deposited after the mid-Miocene Climate Optimum (after 14.2 Ma); in
483 particular, they are characterized by high abundances (up to 39%) of *Selenopemphix*
484 *antarctica*. Even in those intervals, however, the relative abundances of *S. antarctica*
485 do not reach present-day values at the same site (Prebble et al., 2013). The absence of
486 a strong shift towards modern-day-like assemblages in our record can be interpreted
487 to reflect a weaker-than-present ACC. This interpretation is in line with numerical
488 models (Herold et al., 2012; Hill et al., 2013). The ACC itself represents an important
489 barrier for latitudinal surface-water transport towards the Antarctic margin, in
490 addition to the Antarctic Divergence (Olbers et al., 2004). Our data suggest an
491 increase in the influence of oligotrophic dinocysts at the Antarctic margin during the
492 late Oligocene and during the MMCO, which argues against the installation of a
493 vigorous ACC at 30 Ma as recently inferred by Scher et al. (2015): No particular
494 change in sea-surface conditions emerges from our dinoflagellate cyst data around 30
495 Ma, and there is no major change in the benthic $\delta^{18}O$ data either (Figure 5). Instead, if
496 the Tasmanian Gateway had opened to an extent that allowed ACC development
497 (Scher et al., 2015), the ACC must have been much weaker throughout the Oligocene
498 and Miocene than at present, which has also emerged from modelling experiments
499 (Hill et al., 2013). The strongly different dinocyst assemblages compared to present-

day nearby Site U1356 throughout our record imply that a strong coherent ACC was not installed until after the mid-Miocene Climatic Transition (MMCT; 11 Ma). This is consistent with inferences from the lithology at the same site (Salabarnada et al., submitted, this volume), suggesting a proto-ACC much weaker than at present and, likewise, weaker Southern Ocean frontal systems. An alternative explanation is that the ACC increased in strength during the Oligocene–Miocene, but that this strengthening had no influence on the dinocyst assemblages at Site U1356. However, the vigorous nature of the ACC influencing surface as well as bottom waters and governing eddy water circulation in the Southern Ocean (Olbers et al., 2004) in combination with the high sensitivity of dinoflagellates to changes in surface-water conditions (e.g., Zonneveld et al., 2013; Prebble et al., 2013) makes such a scenario very unlikely. Nevertheless, to firmly clarify whether the ACC reached its present-day strength only after the MMCT (as suggested by our data), ocean-circulation modelling of time slices younger than the Oligocene (Hill et al., 2013) will be required.

Our results also seem difficult to reconcile with indications of bottom-water formation at the Wilkes Land margin, as seen from neodymium isotope analyses on the same sediments (Huck et al., 2017). It could be that bottom water formation took place only when surface waters cooled down in wintertime, and the organic proxies are more representative of spring/summer conditions. Salabarnada et al. (this volume) interpret bottom-current activity in the Oligocene at Site U1356 and suggest it may be spilling over from the Ross Sea, like today. Our dinocyst results and the SST reconstructions by Hartman et al. (submitted this volume) suggest that surface waters at the Wilkes Land margin were too warm to allow local bottom-water

formation, therefore our data also supports the suggestion that bottom water along the Wilkes Land margin was sourced from the Ross Sea.

5.3 Implications for ice-sheet and sea-ice variability

The relative abundances of the sea-ice-related *Selenopemphix antarctica* are consistently lower in our record than in present-day dinocyst assemblages nearby Site U1356 (Prebble et al., 2013; Figure 3). This suggests that sea-ice conditions were never similar to today during the studied time interval. More specifically, our dinocysts suggest the occurrence of sea ice near the site only during two time intervals: The first 1.5 million years following the Oi-1 glaciation (33.6–32.1 Ma; Figure 5), and during and after the mid-Miocene climatic Transition (after 14.2 Ma; Figure 5). Numerical ice-sheet/sea-ice modelling (DeConto et al., 2007) has suggested sea-ice to develop only if the continental ice sheets reach the coastline. Our lack of sea-ice indicators during most of the Oligocene and Miocene could thus point towards a much-reduced Antarctic continental ice sheet during that time. The finding of a weaker sea-ice season throughout most of the Oligocene–Miocene at Site U1356 is important because it suggests a decrease in the potential formation of Antarctic bottom waters at this site.

The relative abundance of oligotrophic dinocyst taxa broadly follows long-term Oligocene-Miocene benthic $\delta^{18}O$ trends (see Fig. 5): During times of low $\delta^{18}O$ values in deep-sea benthic foraminifera (and thus high deep-sea temperatures and/or less ice volume; e.g., at 32 Ma, 24 Ma and 15 Ma; Figure 5), the abundance of oligotrophic temperate dinocysts was high (Figure 5). At times of higher $\delta^{18}O$ values, lower deep-sea temperatures and higher ice volume (e.g., at 33.5 Ma, 27 Ma, 23 Ma,

and 13 Ma; Figure 5), temperate dinocysts were reduced in abundance and high-nutrient, sea-ice indicators (re)appeared. Altogether, on long time scales this pattern suggests that there was a stronger influence of warm surface waters at the Wilkes Land margin at times when ice sheets were smaller and climate was warmer, and less influence of warm surface waters during times of larger ice sheets. Hence a connection existed between ice- sheet expansion/retreat and paleoceanography.

Oxygen-isotope mass-balance calculations suggest that a modern-day-sized Antarctic ice sheet formed at the Eocene/Oligocene boundary (DeConto et al., 2008). Benthic $\delta^{18}O$ records suggest that ice sheets must have fluctuated considerably in size during the subsequent Oligocene and Miocene (Liebrand et al., 2017), although this inference lacks an independent assessment of the deep-sea temperature effect in these $\delta^{18}O$ values. The same conclusion was reached based on detailed microfossil, geochemical and facies analyses on sediments from the Gippsland Basin, southeast Australia (Gallagher, et al. 2013). This study suggests that ice volume during the early Oligocene varied by as much as 140–40% of its present-day size, of which the maximum ice volume estimates far exceed those implied by our data. However, there is consistency in the observation of considerable glacial-interglacial and long-term dynamics in the ice-ocean system. This is in contrast to the heavy $\delta^{18}O$ values for Oligocene benthic foraminifera from Maud Rise (ODP Site 690), which lead to suggest Antarctic ice sheets were near-present-day size throughout the Oligocene (Hauptvogel et al., 2017). It remains to be seen whether the variability in paleoceanography as indicated by our data can be extrapolated to larger parts of the Antarctic margin, including regions of deep-water formation. Given the high temperatures and only weak sea-ice influence, the Wilkes Land margin was likely not

571 the primary sector of deep-water formation (see, e.g., Herold et al., 2012), although
572 there is ample evidence for bottom-current activity at the site (Salabarnada et al.,
573 submitted, this volume; Huck et al., 2017). Instead, it appears that bottom-water
574 formation during the Oligocene was taking place along the Wilkes Land coast (Huck,
575 et al. 2017). If the oceanographic and climate variability that we reconstruct offshore
576 Wilkes Land also characterises regions of deep-water formation, some (if not all) of
577 the variability both on long and on orbital time scales as documented in benthic $\delta^{18}O$
578 records would be due to changes in deep-sea temperature rather than Antarctic ice
579 volume (see also Hartman et al., submitted, this volume). Meanwhile, we find little
580 support in our study for the large (and, by implication, marine-terminating)
581 continental ice sheets in this sector of East Antarctica during the Oligocene as implied
582 by Hauptvogel et al. (2017) given the absence of dominance of sea-ice dinocysts and
583 the presence of in situ terrestrial palynomorphs (Strother et al., 2017). As an
584 alternative explanation for the difference in $\delta^{18}O$ values between Maud Rise (Site
585 690) and the equatorial Pacific (Site 1218) during the Oligocene (Hauptvogel et al.,
586 2017), we suggest that these two sedimentary archives have recorded the
587 characteristics of two different deep-water masses, with those at Maud Rise (Site
588 690) being much colder and more saline than those in the equatorial Pacific (Site
589 1218).
590
591 **6. Conclusions**
592 The dinocyst assemblages in the Oligocene–Miocene (33.6–11 Ma) of Site U1356 were
593 interpreted in terms of surface-water paleoceanography via comparison with
594 present-day dinocyst distribution patterns. Based on our results, we suggest that the

Oligocene–Miocene surface paleoceanography of the Southern Ocean was fundamentally different from that of today. A sea-ice signal (yet still weaker than at present) emerges for the Wilkes Land margin only for the first 1.5 million years of the Oligocene (33.6–32.1 Ma) and during and after the mid-Miocene climatic transition (after 14.2 Ma). During the remainder of the Oligocene–Miocene, surface waters off Wilkes Land were warm and relatively oligotrophic; notably, they lack indications of a prominent sea-ice season. Upwelling at the Antarctic Divergence was profoundly weaker during Oligocene and Miocene times than at present, or significantly displaced southward from its present-day position. Furthermore, the continental ice sheets were much reduced at the Wilkes Land sub-glacial basin for most of the Oligocene–Miocene compared to today. The influence of warm oligotrophic surface waters appears strongly coupled to deep-sea $\delta^{18}O$ values, suggesting enhanced low-latitude influence of surface waters during times of light $\delta^{18}O$ in the deep sea and *vice versa*. The absence of (a trend towards a stronger) paleoceanographic isolation of the Wilkes Land margin throughout the Oligocene to mid-Miocene suggests that the ACC may not have attained its full, present-day strength until at least after the mid-Miocene Climatic transition. Moreover, we note considerable glacial-interglacial amplitude variability in this oceanographic setting. Stronger influence of oligotrophic, low-latitude-derived surface waters prevailed over Site U1356 during interglacial times and more eutrophic, colder waters during glacial times. This pattern may suggest considerable latitudinal migration of the AAPF over the course of Oligocene and Miocene glacial-interglacial cycles.

Acknowledgements

This research used data and samples from the Integrated Ocean Drilling Program (IODP). IODP was sponsored by the U.S. National Science Foundation and participating countries under management of Joined Oceanographic Institutions Inc. PKB and FS thank NWO-NNPP grant no 866.10.110, NWO-ALW VENI grant no 863.13.002 for funding and Natasja Welters for technical support. JP acknowledges support through the IODP priority program of the German Research Foundation (DFG). CE and AS thank the Spanish Ministerio de Economía y Competitividad for Grant CTM2014-60451-C2-1-P. We thank Kasia Śliwińska, Stephen Gallagher and an anonymous reviewer for their constructive comments that considerably improved our manuscript.

Author contributions

PKB, FS, CE, and JP designed the research. AJPH, FS and PKB carried out dinocyst analyses for the earliest Oligocene, Miocene, and Oligocene-Miocene boundary interval, respectively. AS and CE provided the lithological data. PKB integrated, cross-validated and compiled the data, and wrote the paper with input from all co-authors.

Figure captions

Figure 1. Paleogeography of the Southwest Pacific Ocean and position of IODP Site U1356 (red star) at (a) 0 Ma, (b) 10 Ma, (c) 20 Ma, and (d) 30 Ma. Figures are modified after Bijl et al. (2018). Reconstructions were adapted from G-plates, with plate circuit from Seton et al. (2012) and absolute plate positions of Torsvik et al. (2012).

Figure 2. Age model for the Oligocene–Miocene interval of Hole U1356A. Core recovery, lithostratigraphic facies after Salabarnada et al. (this volume; see also Sangiorgi et al., 2018) and lithostratigraphic units (Escutia et al., 2011), Samples taken for palynology and age-depth plot (tie points were derived from Tauxe et al., 2012, which has been recalibrated to the GTS2012 time scale of Gradstein et al., 2012 and modified based on Crampton et al., 2016)). Grey intervals in paleomagnetic data reflect unknown paleomagnetic orientation, either due to absence of core recovery or poor signal. (o) = old end; (y) = young end. Figure modified from Bijl et al. (2018).

Figure 3. Generic representation of present-day distributions of dinocysts in surface sediments in the Southern Ocean. The dinocyst pie charts represent average dinocyst assemblage compositions for surface sediments underneath oceanic frontal zones in the Southern Ocean. Figure modified from Sangiorgi et al. (2018), data replotted from Prebble et al. (2013).

Figure 4. Core recovery and lithostratigraphic facies (after Salabarnada et al., this volume, and Sangiorgi et al., 2018) and lithologic units (Escutia et al., 2011),

chronostratigraphic epochs (E = Eocene) and stages (L = Lutetian, Burd. = Burdigalian, Ser. = Serravallian, T. = Tortonian), absolute palynomorph (grey) and in situ dinocyst (black) concentrations (# per gram of dry sediment, presented on a logarithmic scale), palynomorph content (reworked dinocysts, in situ dinocysts, acritarchs, terrestrial palynomorphs (given in percentages of total palynomorphs), and relative abundance of in situ dinocyst eco-groups (in percentage of in situ dinocysts) for the Oligocene–Miocene of Hole U1356A.

Figure 5. Megasplice of benthic foraminiferal oxygen isotope data (De Vleeschouwer et al., 2017) from Site 1146 (Holbourn et al. 2013), Site 1338, (Holbourn et al. 2014), Site 1337 (Holbourn et al., 2015), Site 1090 (Billups et al. 2004), Site 926 (Pälike et al. 2006b) Site 1218 (Pälike et al., 2006a), with a 15-point running mean. In situ dinocyst assemblage data from Site U1356. The age-depth model specified in Figure 2 and Table 1 was used. E. = Eocene, l. = late, P. = Priabonian, T. = Tortonian

Figure 6. Comparison of absolute (left bar, in # * gr $^{-1}$ dry weight) and relative (right bar; in % of total palynomorphs) abundances of palynomorph groups per lithology for Hole U1356A. Average (black lines) and 17–83% percentile (coloured bar) of absolute and relative abundances of total palynomorphs, reworked dinocysts, in situ dinocysts, acritarchs, and terrestrial palynomorphs grouped for the different facies (Salabarnada et al., submitted this volume).

Figure 7. Abundance/concentration of in situ eco-groups within various lithologies at Hole U1356A. Average (black line) and 17–83% percentile (coloured bar) of relative

abundances of grouped taxa from samples from the different facies (Salabarnada et al., submitted this volume).

Table captions

Table 1. Age constraints for the Oligocene–Miocene of Hole U1356A.

Table 2. List of assumed in situ and reworked dinoflagellate cyst taxa encountered in this study. See Bijl et al. (2018) for informal species descriptions and discussion about which species are considered reworked and in situ.

694 References

695 Badger, M. P. S., Lear, C. H., Pancost, R. D., Foster, G. L., Bailey, T. R., Leng, M. J., Abels, H.
696 A.: CO_2 drawdown following the middle Miocene expansion of the Antarctic Ice Sheet,
697 Paleoceanography, 28, 42-53, 2013.

698 Bard, E. and Rickaby, R. E. M.: Migration of the subtropical front as a modulator of glacial
699 climate. Nature. 460, 380-383, 2009.

700 Barker, P., Camerlenghi, A., Acton, G., Brachfeld, S., Cowan, E., Daniels, J., Domack, E., Escutia,
701 C., Evans, A., Eyles, N., Guyodo, Y., Iorio, M., Iwai, M., Kyte, F., Lauer, C., Maldonado, A.,
702 Moerz, T., Osterman, L., Pudsey, C., Schuffert, J., Sjunneskog, C., Vigar, K., Weinheimer, A.,
703 Williams, T., Winter, D., Wolf-Welling, T.: Antarctic glacial history and sea-level change - Leg
704 178 samples Antarctic Peninsula margin sediments, JOIDES Journal 24, 7-10, 1998.

705 Barker, P. F., Barrett, P. J., Cooper, A. K., Huybrechts, P.: Antarctic glacial history from numerical
706 models and continental margin sediments, Palaeogeography, Palaeoclimatology, Palaeoecology,
707 150, 247-267, 1999.

708 Barker, P. F. and Thomas, E.; Origin, signature and paleoclimatic influence of the Antarctic
709 Circumpolar Current, Earth Science Reviews, 66, 143-162, 2004

710 Barrett, P. J.: Antarctic Cenozoic history from the CIROS-1 drillhole, McMurdo Sound. Science
711 Information Publishing Centre DSIR Bulletin, volume 245, Wellington, 1989.

712 Beddow, H. M., Liebrand, D., Sluijs, A., Wade, B. S., Lourens, L. J.: Global change across the
713 Oligocene-Miocene transition: High-resolution stable isotope records from IODP Site U1334
714 (equatorial Pacific Ocean), Paleoceanography, 31, 81-97, 2016.

715 Bijl, P. K., Bendle, A. P. J., Bohaty, S. M., Pross, J., Schouten, S., Tauxe, L., Stickley, C. E.,
716 McKay, R. M., Röhl, U., Olney, M., Sluijs, A., Escutia, C., Brinkhuis, H., Expedition 318
717 scientists; Eocene cooling linked to early flow across the Tasmanian Gateway, Proceedings of the
718 National Academy of Sciences of the United States of America, 110, 9645-9650, 2013a.

719 Bijl, P.K., Houben, A.J.P., Bruls, A., Pross, J., Sangiorgi, F.: Stratigraphic calibration of
720 Oligocene–Miocene organic-walled dinoflagellate cysts from offshore Wilkes Land, East
721 Antarctica, and a zonation proposal: Journal of Micropaleontology, 37(1), pp. 105-138, 2018.

722 Bijl, P.K., Houben, A.J.P., Schouten, S., Bohaty, S.M., Sluijs, A., Reichart, G.J., Sinninghe
723 Damsté, J.S., Brinkhuis, H.: Transient Middle Eocene Atmospheric Carbon Dioxide and
724 Temperature Variations, Science, 330, 819-821, 2010.

725 Bijl, P. K., Pross, J., Warnaar, J., Stickley, C. E., Huber, M., Guerstein, R., Houben, A. J. P., Sluijs,
726 A., Visscher, H., Brinkhuis, H.: Environmental forcings of Paleogene Southern Ocean
727 dinoflagellate biogeography. Paleoceanography, 26, PA1202, 2011.

728 Bijl, P. K., Sluijs, A., Brinkhuis, H.: A magneto- chemo- stratigraphically calibrated dinoflagellate
729 cyst zonation of the early Paleogene South Pacific Ocean. Earth-Science Reviews, 124, 1-31,
730 2013b.

731 Billups, K., Pälike, H., Channell, J. E. T., Zachos, J. C., Shackleton, N. J.: Astronomic calibration
732 of the late Oligocene through early Miocene geomagnetic polarity time scale. Earth and Planetary
733 Science Letters. 224, 33-44, 2004.

734 Boessenkool, K. P., Van Gelder, M., Brinkhuis, H., Troelstra, S. R.: Distribution of organic-walled
735 dinoflagellate cysts in surface sediments from transects across the Polar Front offshore southeast
736 Greenland, J. Quaternary Sci., 16, 661–666, 2001.

737 Brinkhuis, H., Munsterman, D. M., Sengers, S., Sluijs, A., Warnaar, J., Williams, G. L.: Late
738 Eocene to Quaternary dinoflagellate cysts from ODP Site 1168, off western Tasmania, in: Exon,
739 N., Kennett, J. P. (Eds.), Proceedings of the Ocean Drilling Program, Scientific Results, volume
740 189, U.S. Government Printing Office, College Station, Texas, 2003a.

741 Brinkhuis, H., Sengers, S., Sluijs, A., Warnaar, J., Williams, G. L.: Latest Cretaceous to earliest
742 Oligocene, and Quaternary dinoflagellates from ODP Site 1172, East Tasman Plateau, in: Exon, N.,
743 Kennett, J. P. (Eds.), Proceedings of the Ocean Drilling Program, Scientific Results, volume 189.
744 U.S. Government Printing Office, College Station, Texas, 2003b.

745 Close, D. I., Watts, A. B., Stagg, H. M. J.: A marine geophysical study of the Wilkes Land rifted
746 continental margin, Antarctica, Geophysical Journal International, 177, 430-450, 2009.

747 Cook, C. P., Van De Flierdt, T., Williams, T., Hemming, S. R., Iwai, M., Kobayashi, M., Jimenez-
748 Espejo, F. J., Escutia, C., González, J. J., Khim, B., McKay, R. M., Passchier, S., Bohaty, S. M.,
749 Riesselman, C. R., Tauxe, L., Sugisaki, S., Galindo, A. L., Patterson, M. O., Sangiorgi, F., Pierce,
750 E. L., Brinkhuis, H., Klaus, A., Fehr, A., Bendle, J. A. P., Bijl, P. K., Carr, S. A., Dunbar, R. B.,
751 Flores, J. A., Hayden, T. G., Katsuki, K., Kong, G. S., Nakai, M., Olney, M. P., Pekar, S. F., Pross,
752 J., Röhl, U., Sakai, T., Shrivastava, P. K., Stickley, C. E., Tuo, S., Welsh, K., Yamane, M.:
753 Dynamic behaviour of the East Antarctic ice sheet during Pliocene warmth, Nature Geoscience, 6,
754 765-769, 2013.

755 Cooper, A. K. and O'Brien, P. E.: Leg 188 synthesis: Transitions in the glacial history of the Prydz
756 Bay region, East Antarctica, from ODP drilling, Proceedings of the Ocean Drilling Program:
757 Scientific Results, 188, 1-42, 2004.

758 Crampton, J. S., Cody, R. D., Levy, R., Harwood, D., McKay, R., Naish, T. R.: Southern Ocean
759 phytoplankton turnover in response to stepwise Antarctic cooling over the past 15 million years.
760 Proceedings of the National Academy of Sciences of the United States of America, 113, 6868-
761 6873, 2016.

762 DeConto, R. M., Pollard, D., Harwood, D.: Sea-ice feedback and Cenozoic evolution of Antarctic
763 climate and ice sheets, Paleoceanography, 22, PA3214, 2007.

764 DeConto, R. M., Pollard, D., Wilson, P. A., Pälike, H., Lear, C. H., Pagani, M.: Thresholds for
765 Cenozoic bipolar glaciation, Nature, 455, 652-657, 2008.

766 Egger, L. M., Bahr, A., Friedrich, O., Wilson, P. A., Norris, R. D., van Peer, T. E., Lippert, P. C.,
767 Liebrand, D., Pross, J.: Sea-level and surface-water change in the western North Atlantic across the
768 Oligocene–Miocene Transition: a palynological perspective from IODP Site U1406 (New-
769 foundland margin), Marine Micropaleontology, 139, 57-71, 2018.

770 Escutia, C., Brinkhuis, H.: From Greenhouse to Icehouse at the Wilkes Land Antarctic Margin:
771 IODP Expedition 318 Synthesis of Results, Developments in Marine Geology, 7, pp. 295-328,
772 2014.

773 Escutia, C., Brinkhuis, H., Klaus, A. and Expedition 318 Scientists; Proceedings of the Integrated
774 Ocean Drilling Program, Initial Results, volume 318, Tokyo (Integrated Ocean Drilling Program
775 Management International, Inc.), 2011.

776 Esper, O. and Zonneveld, K. A. F.: The potential of organic-walled dinoflagellate cysts for the
777 reconstruction of past sea-surface conditions in the Southern Ocean, Marine Micropaleontology,
778 65, 185-212, 2007.

779 Esper, O. and Zonneveld, K. A. F.: Distribution of organic-walled dinoflagellate cysts in surface
780 sediments of the Southern Ocean (eastern Atlantic sector) between the Subtropical Front and the
781 Weddell Gyre, Marine Micropaleotology, 46, 177-208, 2002.

Exon, N. F., Kennet, J. P., Malone, M.: Leg 189 Synthesis: Cretaceous- Holocene history of the Tasmanian Gateway. In Exon, N.F., Kennett, J.P., and Malone, M.J. (Eds.), Proceedings of the Ocean Drilling Program, Scientific Results, Volume 189, 2004.

Eynaud, F., Giraudeau, J., Pichon, J., Pudsey, C. J.: Sea-surface distribution of coccolithophores, diatoms, silicoflagellates and dinoflagellates in the South Atlantic Ocean during the late austral summer 1995, Deep-Sea Research Part I: Oceanographic Research Papers, 46, 451-482, 1999.

Foster, G. L., Lear, C. H., Rae, J. W. B.: The evolution of pCO_2, ice volume and climate during the middle Miocene, Earth and Planetary Science Letters, 341-344, 243-254, 2012.

Foster, G. L. and Rohling, E. J.: Relationship between sea level and climate forcing by CO_2 on geological timescales, Proceedings of the National Academy of Sciences of the United States of America, 110, 1209-1214, 2013.

Fretwell, P., Pritchard, H. D., Vaughan, D. G., Bamber, J. L., Barrand, N. E., Bell, R., Bianchi, C., Bingham, R. G., Blankenship, D. D., Casassa, G., Catania, G., Callens, D., Conway, H., Cook, A. J., Corr, H. F. J., Damaske, D., Damm, V., Ferraccioli, F., Forsberg, R., Fujita, S., Gim, Y., Gogineni, P., Griggs, J. A., Hindmarsh, R. C. A., Holmlund, P., Holt, J.W., Jacobel, R. W., Jenkins, A., Jokat, W., Jordan, T., King, E. C., Kohler, J., Krabill, W., Riger-Kusk, M., Langley, K. A., Leitchenkov, G., Leuschen, C., Luyendyk, B. P., Matsuoka, K., Mouginot, J., Nitsche, F. O., Nogi, Y., Nost, O. A., Popov, S.V., Rignot, E., Rippin, D. M., Rivera, A., Roberts, J., Ross, N., Siegert, M. J., Smith, A.M., Steinhage, D., Studinger, M., Sun, B., Tinto, B.K., Welch, B.C., Wilson, D., Young, D. A., Xiangbin, C., Zirizzotti, A.: Bedmap2: Improved ice bed, surface and thickness datasets for Antarctica, Cryosphere, 7, 375-393, 2013.

Gallagher, S. J., Villa, G., Drysdale, R. N., Wade, B. S., Scher, H., Li, Q., Wallace, M. W., Holdgate, G. R.: A near-field sea level record of east Antarctic ice sheet instability from 32 to 27 Myr. Paleoceanography. 28, 1-13, 2013.

Gradstein, F. M., Ogg, J. G., Schmitz, M. D., Ogg, G. M.: The Geologic Time Scale 2012, 1-2, 1-1144, Elsevier, Amsterdam, the Netherlands, 2012.

Gradstein, F. M., Ogg, J. G., Smith, A. G.: A geologic timescale 2004, Cambridge University Press, Cambridge, 2004.

Greenop, R., Foster, G. L., Wilson, P. A., Lear, C. H.: Middle Miocene climate instability associated with high-amplitude CO_2 variability, Paleoceanography, 29, 845-853, 2014.

Hartman, J. D., Sangiorgi, F., Salabarnada, A., Peterse, F., Houben, A. J. P., Schouten, S., Escutia, C., and Bijl, P. K.: Oligocene TEX_{86}-derived seawater temperatures from offshore Wilkes Land (East Antarctica), Clim. Past Discuss., https://doi.org/10.5194/cp-2017-153, in review, 2017.

Harland, R. and Pudsey, C. J.:Dinoflagellate cysts from sediment traps deployed in the Bellingshausen, Weddell and Scotia seas, Antarctica. Marine Micropaleontology. 37, 77-99, 1999..

Harwood, D., Levy, R., Cowie, J., Florindo, F., Naish, T., Powell, R., Pyne, A.: Deep drilling with the ANDRILL program in Antarctica, Scientific Drilling, 1, 43-45, 2006.

Hauptvogel, D. W., Pekar, S. F., Pincay, V.: Evidence for a heavily glaciated Antarctica during the late Oligocene "warming" (27.8-24.5): stable isotope records from ODP Site 690, Paleoceanography, PA002972, 384-384-396, 2017.

Herold, N., Huber, M., Müller, R. D.: Modeling the Miocene Climatic Optimum. Part I: Land and atmosphere, Journal of Climate 24, 6353-6373, 2011.

Herold, N., Huber, M., Müller, R. D., Seton, M.: Modeling the Miocene Climatic Optimum: Ocean circulation, Paleoceanography 27, PA1209, 2012.

826 Hill, D. J., Haywood, A. M., Valdes, P. J., Francis, J. E., Lunt, D. J., Wade, B. S., Bowman, V. C.:
827 Paleogeographic controls on the onset of the Antarctic circumpolar current, Geophysical Research
828 Letters, 40, 5199-5204, 2013.

829 Holbourn, A., Kuhnt, W., Clemens, S., Prell, W., Andersen, N.: Middle to late Miocene stepwise
830 climate cooling: Evidence from a high-resolution deep water isotope curve spanning 8 million
831 years. Paleoceanography. 28, 688-699, 2013.

832 Holbourn, A., Kuhnt, W., Lyle, M., Schneider, L., Romero, O., Andersen, N.: Middle Miocene
833 climate cooling linked to intensification of eastern equatorial Pacific upwelling. Geology. 42, 19-
834 22, 2014

835 Holbourn, A., Kuhnt, W., Kochhann, K. G. D., Andersen, N., Meier, K. J.: Global perturbation of
836 the carbon cycle at the onset of the Miocene Climatic Optimum, Geology, 43, 123-126, 2015.

837 Houben, A. J. P.: Triggers and Consequences of glacial expansion across the Eocene-Oligocene
838 transition. LPP contributions series no. 39, PhD thesis Utrecht University, Utrecht, the Netherlands,
839 2012.

840 Houben, A. J. P., Bijl, P. K., Pross, J., Bohaty, S. M., Passchier, S., Stickley, C. E., Röhl, U.,
841 Sugisaki, S., Tauxe, L., Van De Flierdt, T., Olney, M., Sangiorgi, F., Sluijs, A., Escutia, C.,
842 Brinkhuis, H.: Reorganization of Southern Ocean plankton ecosystem at the onset of Antarctic
843 glaciation, Science, 340, 341-344, 2013.

844 Huck, C. E., van de Flierdt, T., Bohaty, S. M., Hammond, S. J.: Antarctic climate, Southern Ocean
845 circulation patterns, and deep water formation during the Eocene. Paleoceanography. 32, 674-691,
846 2017

847 IPCC: Climate Change 2013: The Physical Science Basis. Contribution of Working Group I to the
848 Fifth Assessment Report of the Intergovernmental Panel on Climate Change, Cambridge
849 University Press, Cambridge, United Kingdom and New York, NY, USA, 2013.

850 Knorr, G. and Lohmann, G.: Climate warming during Antarctic ice sheet expansion at the middle
851 Miocene transition. Nature Geoscience, 7, 376-381, 2014.

852 Kohfeld, K. E., Graham, R. M., de Boer, A. M., Sime, L. C., Wolff, E. W., Le Quéré, C., Bopp, L.
853 Southern Hemisphere westerly wind changes during the Last Glacial Maximum: paleo-data
854 synthesis, Quaternary Science Reviews, 68, 76-95, 2013.

855 Lear, C. H., Rosenthal, Y. Coxall, H. K., Wilson, P. A. Late Eocene to early Miocene ice sheet
856 dynamics and the global carbon cycle, *Paleoceanography*, 19, PA4015, doi:
857 10.1029/2004PA001039, 2004.

858 Levy, R. H., Harwood, D. M.: Tertiary marine palynomorphs from the McMurdo Sound erratics,
859 Antarctica, in: Stilwell, J. D., Feldmann, R. M. (Eds.), Paleobiology and Paleoenvironments of
860 Eocene rocks, McMurdo Sound, East Antarctica, AGU Antarctic Research Series, pp. 183-242,
861 2000.

862 Liebrand, D., de Bakker, A. T. M., Beddow, H. M., Wilson, P. A., Bohaty, S. M., Ruessink, G.,
863 Pälike, H., Batenburg, S. J., Hilgen, F. J., Hodell, D. A., Huck, C. E., Kroon, D., Raffi, I., Saes, M.
864 J. M., van Dijk, A. E., Lourens, L. J.: Evolution of the early Antarctic ice ages, PNAS, 110(15),
865 3867-3872, 2017.

866 Liebrand, D., Lourens, L. J., Hodell, D. A., De Boer, B., Van De Wal, R. S. W., Pälike, H.:
867 Antarctic ice sheet and oceanographic response to eccentricity forcing during the early Miocene,
868 Climate of the Past, 7, 869-880, 2011.

869 Marret, F. and De Vernal, A., 1997. Dinoflagellate cyst distribution in surface
870 sediments of the southern Indian Ocean. Marine Micropaleontology. 29, 367-392.

871 Olbers, D., Borowski, D., Völker, C., Wölff, J.: The dynamical balance, transport and circulation of
872 the Antarctic Circumpolar Current. Antarctic Science, 16, 439-470, 2004.

873 Pälike, H., Norris, R. D., Herrle, J. O., Wilson, P. A., Coxall, H. K., Lear, C. H., Shackleton, N. J.,
874 Tripati, A. K., Wade, B. S.: The Heartbeat of the Oligocene Climate System, Science, 314, 1894-
875 1898, 2006a.

876 Pälike, H., Frazier, J., Zachos, J. C.: Extended orbitally forced palaeoclimatic records from the
877 equatorial Atlantic Ceara Rise. Quaternary Science Reviews. 25, 3138-3149, 2006b

878 Prebble, J. G., Crouch, E. M., Carter, L., Cortese, G., Bostock, H., Neil, H.: An expanded modern
879 dinoflagellate cyst dataset for the Southwest Pacific and Southern Hemisphere with environmental
880 associations, Marine Micropaleontology, 101, 33-48, 2013.

881 Rignot, E., Jacobs, S., Mouginot, J., Scheuchl, B.: Ice-shelf melting around Antarctica. Science,
882 341, 266-270, 2013.

883 Robert, C., Anderson, J., Armienti, P., Atkins, C., Barrett, P., Bohaty, S., Bryce, S., Claps, M.,
884 Curran, M., Davey, F. J., De Santis, L., Ehrmann, W., Florindo, F., Fielding, C., Hambrey, M.,
885 Hannah, M., Harwood, D. M., Henrys, S., Hoelscher, F., Howe, J. A., Jarrard, R., Kettler, R.,
886 Kooyman, S., Kopsch, C., Krissek, L., Lavelle, M., Levac, E., Niessen, F., Passchier, S., Paulsen,
887 T., Powell, R., Pyne, A., Rafat, G., Raine, I. J., Roberts, A. P., Sagnotti, L., Sandroni, S., Scholz,
888 E., Simes, J., Smellie, J., Strong, P., Tabecki, M., Talarico, F.M., Taviani, M., Verosub, K. L.,
889 Villa, G., Webb, P. N., Wilson, G. S., Wilson, T., Wise, S. W., Wonik, T., Woolfe, K., Wrenn, J.
890 H.: Summary of Results from CRP-1, Cape Roberts Project, Antarctica, Terra Antarctica, 5, 125-
891 137, 1998.

892 Rovere, A., Raymo, M. E., Mitrovica, J. X., Hearty, P. J., O'Leary, M. J., Inglis, J. D.: The Mid-
893 Pliocene sea-level conundrum: Glacial isostasy, eustasy and dynamic topography, Earth and
894 Planetary Science Letters, 387, 27-33, 2014.

895 Salabarnada, A., Escutia, C., Röhl, U., Nelson, C. H., McKay, R., Jiménez-Espejo, F. F., Bijl, P.
896 K., Hartman, J. D., Ikehara, M., Strother, S. L., Salzmann, U., Evangelinos, D., López-Quirós, A.,
897 Flores, J. A., Sangiorgi, F., and Brinkhuis, H.: Late Oligocene obliquity-paced contourite
898 sedimentation in the Wilkes Land margin of East Antarctica: implications for paleoceanographic
899 and ice sheet configurations, Clim. Past Discuss., https://doi.org/10.5194/cp-2017-152, in review,
900 2017..

901 Sangiorgi, F., Bijl, P.K., Passchier, S., Salzmann, U., Schouten, S., McKay, R., Cody, R. D., Pross,
902 J., Van De Flierdt, T., Bohaty, S. M., Levy, R., Williams, T., Escutia, C., Brinkhuis, H.: Southern
903 Ocean warming and Wilkes Land ice sheet retreat during the mid-Miocene, Nature
904 Communications, 9 (1), art. no. 317, 2018.

905 Scher, H. D. and Martin, E. M.: Circulation in the Southern Ocean during the Paleogene inferred
906 from neodymium isotopes. Earth and Planetary Science Letters, 228, 391-405, 2004.

907 Scher, H. D., Whittaker, J. M., Williams, S. E., Latimer, J. C., Kordesch, W. E. C., Delaney, M. L.:
908 Onset of Antarctic Circumpolar Current 30 million years ago as Tasmanian Gateway aligned with
909 westerlies, Nature, 523, 580-583, 2015.

910 Seton, M., Müller, R.D., Zahirovic, S., Gaina, C., Torsvik, T., Shephard, G., Talsma, A., Gurnis,
911 M., Turner, M., Maus, S., Chandler, M.: Global continental and ocean basin reconstructions since
912 200Ma, Earth-Science Reviews, 113, 212-270, 2012.

913 Shepherd, A., Ivins, E. R., Geruo, A., Barletta, V. R., Bentley, M. J., Bettadpur, S., Briggs, K. H.,
914 Bromwich, D. H., Forsberg, R., Galin, N., Horwath, M., Jacobs, S., Joughin, I., King, M. A.,
915 Lenaerts, J. T. M., Li, J., Ligtenberg, S. R. M., Luckman, A., Luthcke, S.B., McMillan, M.,
916 Meister, R., Milne, G., Mouginot, J., Muir, A., Nicolas, J. P., Paden, J., Payne, A. J., Pritchard, H.,
917 Rignot, E., Rott, H., Sørensen, L. S., Scambos, T. A., Scheuchl, B., Schrama, E. J. O., Smith, B.,
918 Sundal, A. V., Van Angelen, J. H., Van De Berg, W. J., Van Den Broeke, M. R., Vaughan, D. G.,
919 Velicogna, I., Wahr, J., Whitehouse, P. L., Wingham, D. J., Yi, D., Young, D., Zwally, H. J.: A
920 reconciled estimate of ice-sheet mass balance, Science, 338, 1183-1189, 2012.

921 Sluijs, A., Brinkhuis, H., Stickley, C. E., Warnaar, J., Williams, G. L., Fuller, M.: Dinoflagellate
922 cysts from the Eocene - Oligocene transition in the Southern Ocean: Results from ODP Leg 189,
923 in: Exon, N., Kennett, J. P. (Eds.), Proceedings of the Ocean Drilling Program, Scientific Results,
924 volume 189, U.S. Government Printing Office, College Station, Texas, USA, 2003.

925 Sluijs, A., Pross, J., Brinkhuis, H.: From greenhouse to icehouse; organic walled dinoflagellate
926 cysts as paleoenvironmental indicators in the Paleogene, Earth-Science Reviews, 68, 281-315,
927 2005.

928 Stocchi, P., Escutia, C., Houben, A.J.P., Vermeersen, B.L.A., Bijl, P.K., Brinkhuis, H., DeConto,
929 R.M., Galeotti, S., Passchier, S., Pollard, D., Klaus, A., Fehr, A., Williams, T., Bendle, J.A.P.,
930 Bohaty, S.M., Carr, S.A., Dunbar, R.B., Flores, J.A., Gonzàlez, J.J., Hayden, T.G., Iwai, M.,
931 Jimenez-Espejo, F.J., Katsuki, K., Kong, G.S., McKay, R.M., Nakai, M., Olney, M.P., Pekar, S.F.,
932 Pross, J., Riesselman, C., Röhl, U., Sakai, T., Shrivastava, P.K., Stickley, C.E., Sugisaki, S., Tauxe,
933 L., Tuo, S., Van De Flierdt, T., Welsh, K., Yamane, M. Relative sea-level rise around East
934 Antarctica during Oligocene glaciation. Nature Geoscience, 6 (5), pp. 380-384, doi:
935 10.1038/ngeo1783, 2013.

936 Storkey, C. A.: Distribution of marine palynomorphs in surface sediments, Prydz Bay, Antarctica.
937 MSc thesis Victoria University of Wellington, New Zealand. http://hdl.handle.net/10063/21, 2006.

938 Strother, S. L., Salzmann, U., Sangiorgi, F., Bijl, P. K., Pross, J., Escutia, C., Salabarnada, A.,
939 Pound, M. J., Voss, J., Woodward, J.: A new quantitative approach to identify reworking in Eocene
940 to Miocene pollen records from offshore Antarctica using red fluorescence and digital imaging,
941 Biogeosciences, 14, 2089-2100, 2017.

942 Tauxe, L., Stickley, C. E., Sugisaki, S., Bijl, P. K., Bohaty, S., Brinkhuis, H., Escutia, C., Flores, J.
943 A., Iwai, M., Jimenez-Espejo, F., McKay, R., Passchier, S., Pross, J., Riesselman, C., Röhl, U.,
944 Sangiorgi, F., Welsh, K., Klaus, A., Bendle, J. A. P., Dunbar, R., Gonzalez, J., Olney, M. P., Pekar,
945 S. F., van de Flierdt, T.: Chronostratigraphic framework for the IODP Expedition 318 cores from
946 the Wilkes Land Margin: constraints for paleoceanographic reconstruction, Paleoceanography, 27,
947 PA2214, 2012.

948 Torsvik, T. H., Van der Voo, R., Preeden, U., Niocaill, C. M., Steinberger, B., Doubrovine, P. V.,
949 van Hinsbergen, D. J. J., Domeier, M., Gaina, C., Tohver, E., Meert, J. G., McCausland, P. J.,
950 Cocks, L. R. M.: Phanerozoic polar wander, palaeogeography and dynamics. Earth-Science
951 Reviews, 114, 325-368, 2012.

952 Van Hinsbergen, D. J. J., De Groot, L. V., Van Schaik, S. J., Spakman, W., Bijl, P. K., Sluijs, A.,
953 Langereis, C. G., Brinkhuis, H.: A paleolatitude calculator for paleoclimate studies. PLoS ONE,
954 10(6), e0126946, 2015.

955 Wilson, G. S., Bohaty, S. M., Fielding, C. R., Florindo, F., Hannah, M.J., Hardwood, D. M.,
956 Mcintosh, W.C., Naish, T. R., Roberts, A. P., Sagnotti, L., Scherer, R. P. , Strong, C. P., Verosub,
957 K. L., Villa, G., Webb, P. -., Woolfe, K. J.: Chronostratigraphy of CRP-2/2A, Victoria Land Basin,
958 Antarctica, Terra Antarctica 7, 647-654, 2000.

959 Wise, S. W. and Schlich, R.,. Proceedings of the Ocean Drilling Program, Scientific Results,
960 volume 120, U.S. Government Printing Office, College Station, Texas, 1992.

961 Wouters, B., Martin-Español, A., Helm, V., Flament, T., van Wessem, J. M., Ligtenberg, S. R. M.,
962 van den Broeke, M. R., Bamber, J. L.: Dynamic thinning of glaciers on the Southern Antarctic
963 Peninsula, Science 348 (6237), 899-903, 2015.

964 Wrenn, J.H. and Hart, G.F.: Paleogene dinoflagellate cyst biostratigraphy of Seymour Island,
965 Antarctica, Geological Society of America Memoires, 169, 321-447, 1988.

966 Xiao, W., Esper, O., Gersonde, R.: Last Glacial - Holocene climate variability in the Atlantic sector
967 of the Southern Ocean. Quaternary Science Reviews. 135, 115-137, 2016.

968 Zachos, J. C., Dickens, G. R., Zeebe, R. E.: An early Cenozoic perspective on greenhouse warming
969 and carbon-cycle dynamics, Nature 451, 279-283, 2008.

970 Zevenboom, D.: Dinoflagellate cysts from the Mediterranean late Oligocene and Miocene, PhD
971 thesis Utrecht University, Utrecht, the Netherlands, 1995.

972 Zonneveld, K. A. F., Marret, F., Versteegh, G. J. M., Bogus, K., Bonnet, S., Bouimetarhan, I.,
973 Crouch, E., de Vernal, A., Elshanawany, R., Edwards, L., Esper, O., Forke, S., Grøsfjeld, K.,
974 Henry, M., Holzwarth, U., Kielt, J., Kim, S., Ladouceur, S., Ledu, D., Chen, L., Limoges, A.,
975 Londeix, L., Lu, S., Mahmoud, M. S., Marino, G., Matsouka, K., Matthiessen, J., Mildenhall, D.
976 C., Mudie, P., Neil, H.L., Pospelova, V., Qi, Y., Radi, T., Richerol, T., Rochon, A., Sangiorgi, F.,
977 Solignac, S., Turon, J., Verleye, T., Wang, Y., Wang, Z., Young, M.: Atlas of modern
978 dinoflagellate cyst distribution based on 2405 data points, Review of Palaeobotany and Palynology,
979 191, 1-197, 2013.

980

Fig. 1

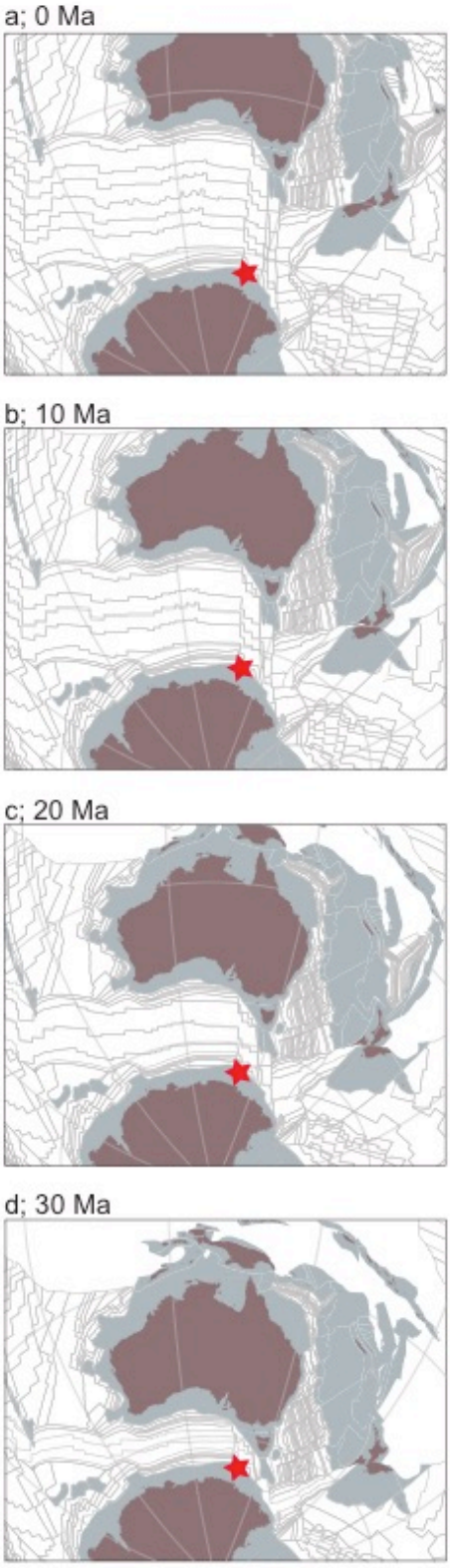

981

982

983

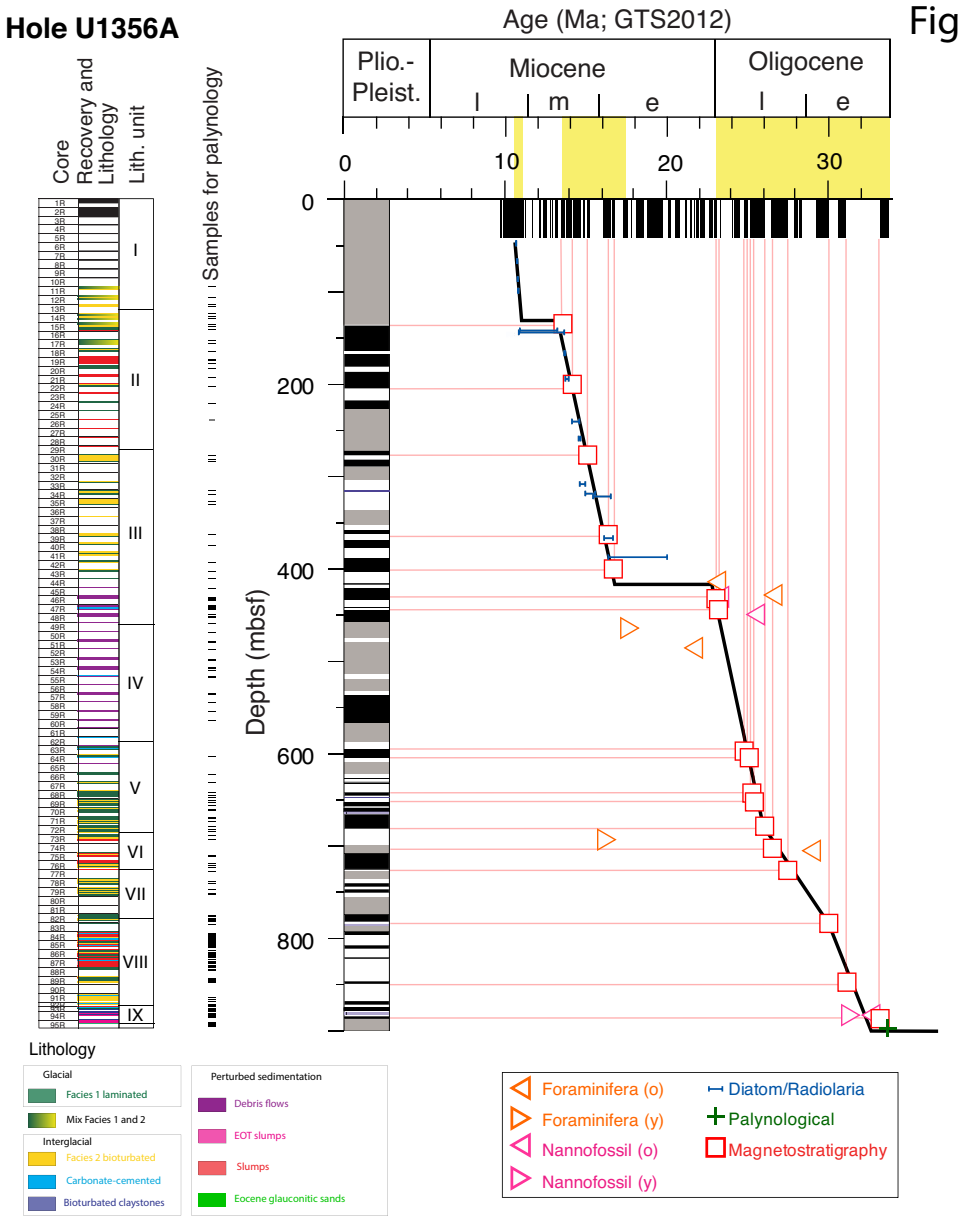
Hole U1356A
Age (Ma; GTS2012)
Plio.-Pleist.
Miocene
Oligocene
l
m
e
l
e
0
10
20
30
Core
Recovery and Lithology
Lith. unit
Samples for palynology
I
II
III
IV
V
VI
VII
VIII
IX
Depth (mbsf)
0
200
400
600
800
Lithology
Glacial
Facies 1 laminated
Mix Facies 1 and 2
Interglacial
Facies 2 bioturbated
Carbonate-cemented
Bioturbated claystones
Perturbed sedimentation
Debris flows
EOT slumps
Slumps
Eocene glauconitic sands
Foraminifera (o)
Foraminifera (y)
Nannofossil (o)
Nannofossil (y)
Diatom/Radiolaria
Palynological
Magnetostratigraphy

Fig. 2

984


Fig. 3
120°W
150°W
180°
30°S
90°W
150°E
30°S
STF
SAF
AAPF
U1356
60°W
60°S
60°S
Oceanic fronts
AAPF Antarctic Polar Front
SAF Sub-Antarctic Front
STF Sub-Tropical Front
Dinocysts
Selenopemphix antarctica
Other protoperidinioideae
Impagidinium spp.
Nematosphaeropsis labyrinthus
Operculodinium spp.
Other gonyaulacoideae

985

986

Fig. 4

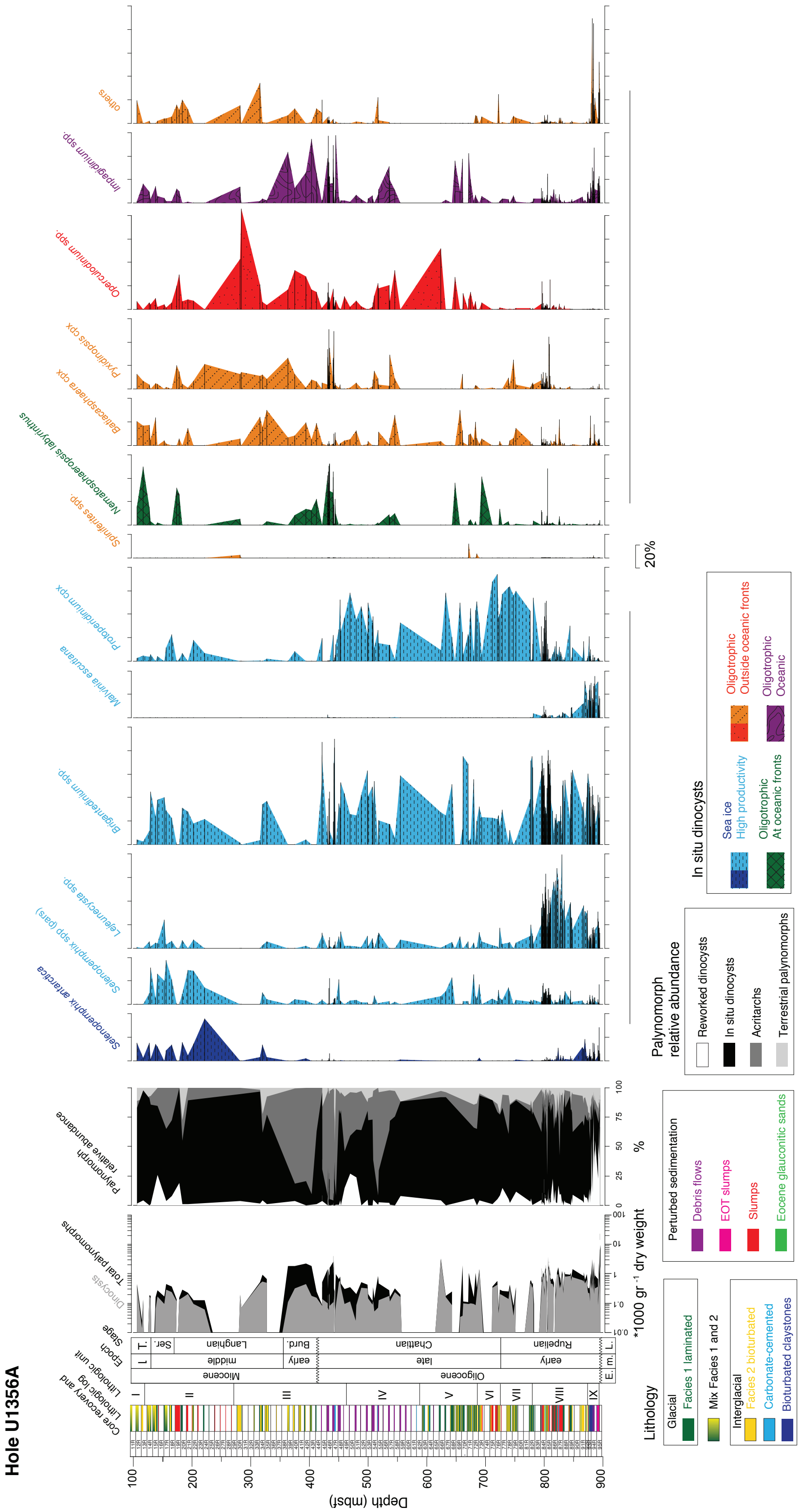
Hole U1356A
Depth (mbsf)
100
200
300
400
500
600
700
800
900
Core recovery and Lithologic log
Lithologic unit
Epoch
Stage
I
II
III
IV
V
VI
VII
VIII
IX
Miocene
Oligocene
l.
middle
early
late
early
E.
m.
T.
Ser.
Langhian
Burd.
Chattian
Rupelian
L.
Dinocysts
Total palynomorphs
0.01
0.1
1
10
100
*1000 gr -1 dry weight
Palynomorph relative abundance
0
25
50
75
100
%
Selenopemphix antarctica
Selenopemphix spp (pars)
Lejeunecysta spp.
Brigantedinium spp.
Malvinia escutiana
Protoperidinium cpx
Spiniferites spp.
Nematosphaeropsis labyrinthus
Batiacasphaera cpx
Pyxidinopsis cpx
Operculodinium spp.
Impagidinium spp.
others
20%
Lithology
Glacial
Facies 1 laminated
Mix Facies 1 and 2
Interglacial
Facies 2 bioturbated
Carbonate-cemented
Bioturbated claystones
Perturbed sedimentation
Debris flows
EOT slumps
Slumps
Eocene glauconitic sands
Palynomorph relative abundance
Reworked dinocysts
In situ dinocysts
Acritarchs
Terrestrial palynomorphs
In situ dinocysts
Sea ice
High productivity
Oligotrophic
At oceanic fronts
Oligotrophic
Outside oceanic fronts
Oligotrophic
Oceanic

989

990

Fig. 5

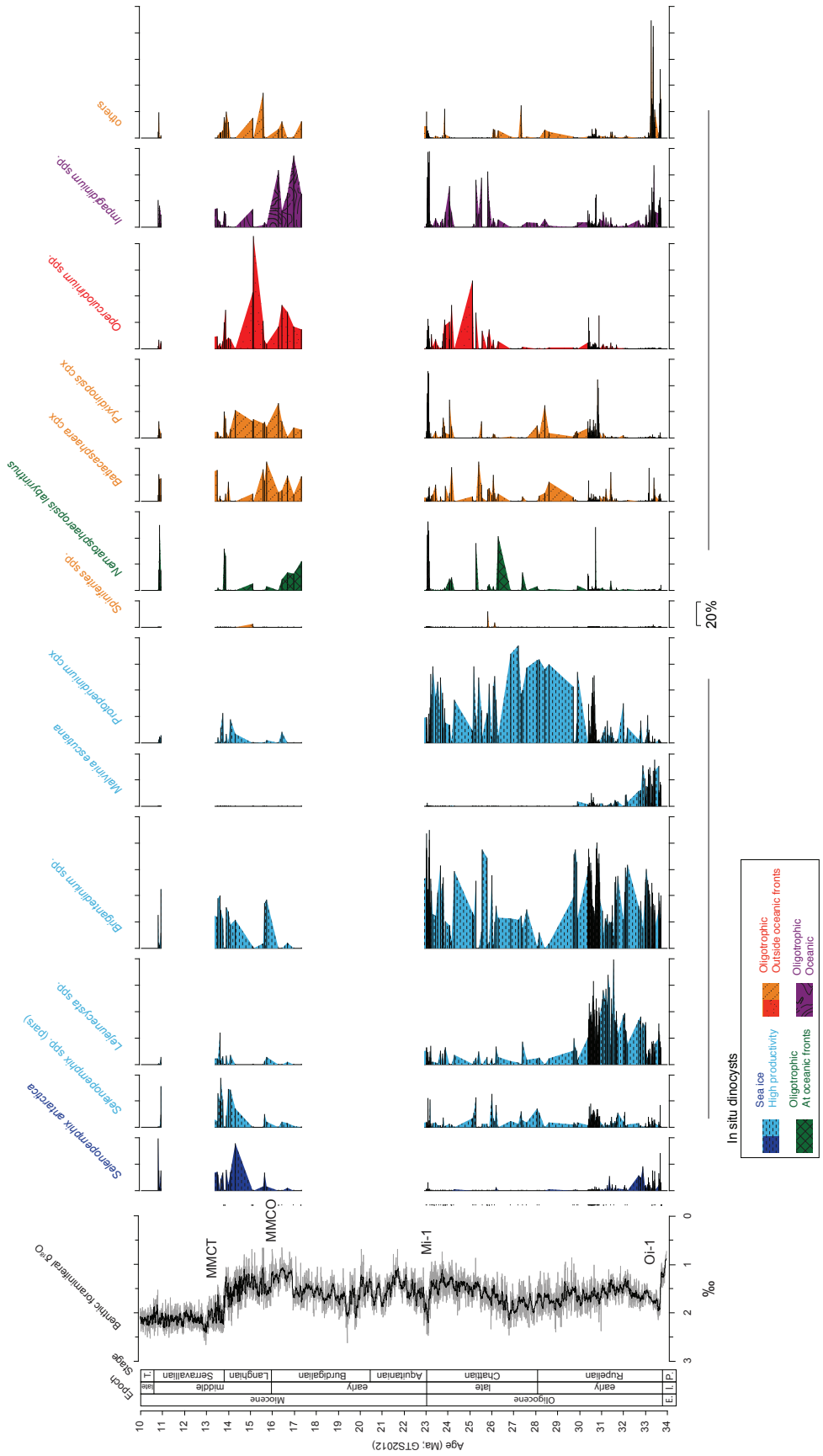
Age (Ma; GTS2012)
Epoch
Stage
Benthic foraminiferal δ18O
‰
MMCT
MMCO
Mi-1
Oi-1
Oligocene
Miocene
Rupelian
Chattian
Aquitanian
Burdigalian
Langhian
Serravallian
Sea ice
High productivity
Oligotrophic
At oceanic fronts
Oligotrophic
Outside oceanic fronts
Oligotrophic
Oceanic
In situ dinocysts
20%
Selenopemphix antarctica
Selenopemphix spp. (pars)
Lejeunecysta spp.
Brigantedinium spp.
Malvinia escutiana
Protoperidinium cpx
Spiniferites spp.
Nematosphaeropsis labyrinthus
Batiacasphaera cpx
Pyxidinopsis cpx
Operculodinium spp.
Impagidinium spp.
others

Fig. 6

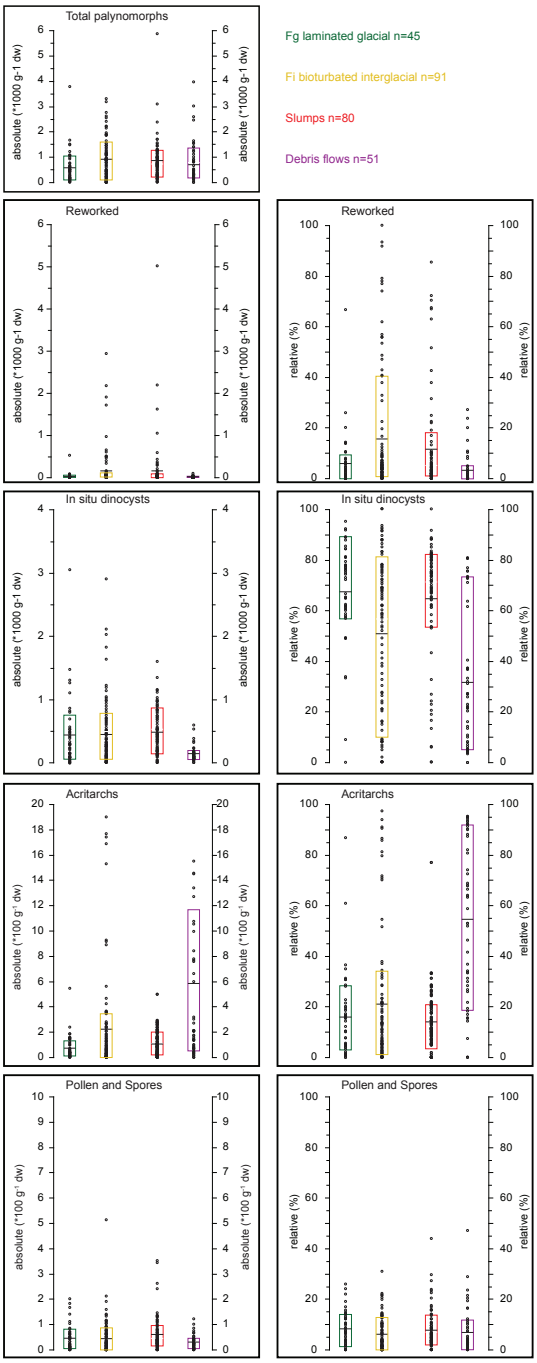
Total palynomorphs
Reworked
Reworked
In situ dinocysts
In situ dinocysts
Acritarchs
Acritarchs
Pollen and Spores
Pollen and Spores
absolute (*1000 g-1 dw)
relative (%)
absolute (*100 g-1 dw)
Fg laminated glacial n=45
Fi bioturbated interglacial n=91
Slumps n=80
Debris flows n=51

991

Fig. 7

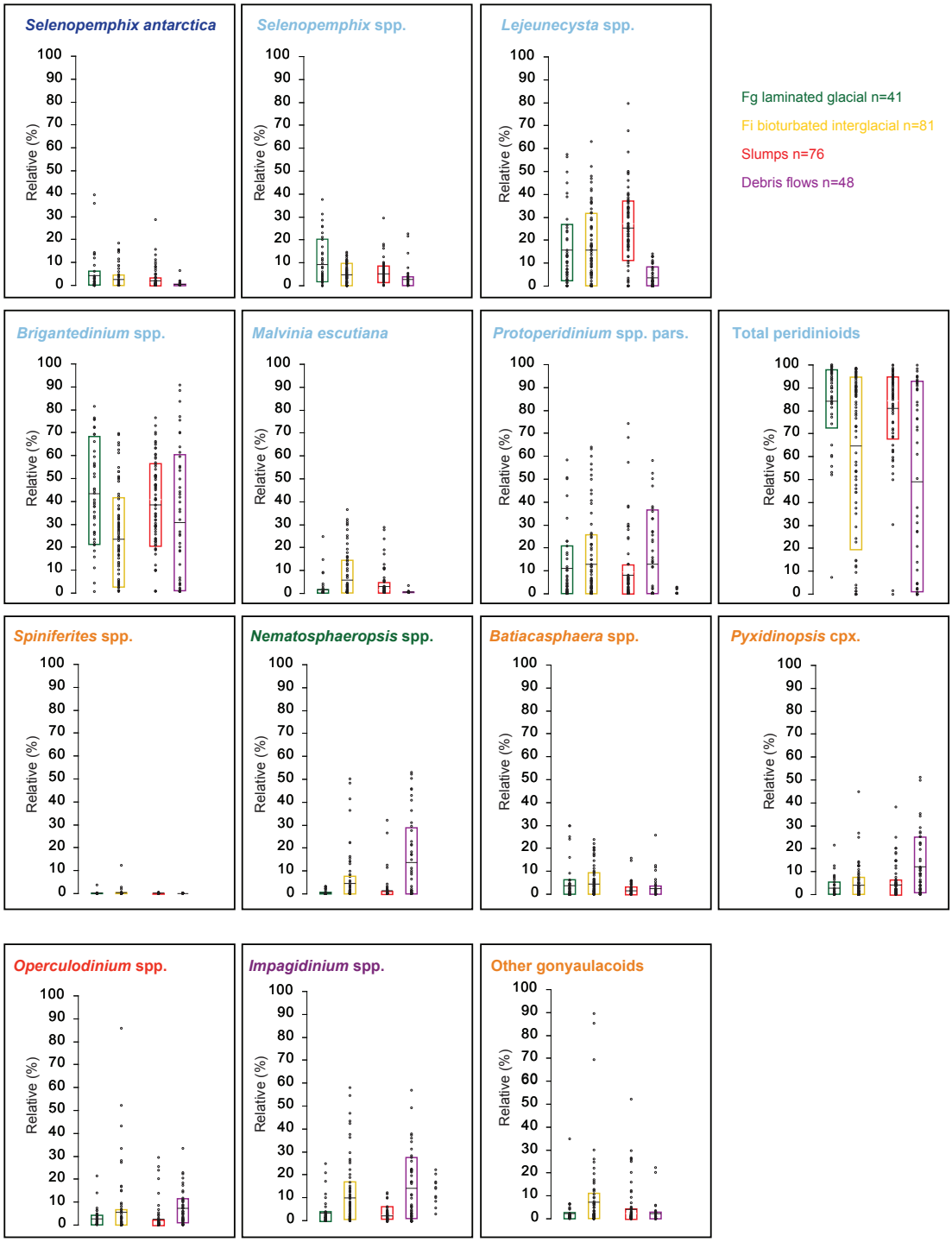
Selenopemphix antarctica
Selenopemphix spp.
Lejeunecysta spp.
Brigantedinium spp.
Malvinia escutiana
Protoperidinium spp. pars.
Total peridinioids
Spiniferites spp.
Nematosphaeropsis spp.
Batiacasphaera spp.
Pyxidinopsis cpx.
Operculodinium spp.
Impagidinium spp.
Other gonyaulacoids
Relative (%)
0
10
20
30
40
50
60
70
80
90
100
Fg laminated glacial n=41
Fi bioturbated interglacial n=81
Slumps n=76
Debris flows n=48

992

Table 1

type	FO/LO	Genus, chror	(Gradstein 20	top core	top interval	bottom core	bottom inter	depth averag	error
CONOP			10.76					98.66	
CONOP			10.92					133.80	
CONOP			13.41					133.81	
PM	(o)	C5ACn	14.07	22R-2,	75	22R-2,	90	203.23	0.07
PM	(y)	C5Bn.2n	15.03	30R-2,	50	30R-2,	75	279.63	0.13
PM	(o)	C5Cn.1n	16.27	39R-1,	35	39R-1,	65	364.10	0.15
PM	(o)	C5Cn.3n	16.72	42R-2,	59	43R-1,	25	398.28	3.98
			17.50	44R-CC		45R-CC		416.90	
			23.00	44R-CC		45R-CC		416.91	
PM	(o)	C6Cn.2n	23.03	45R-CC	40	46R-1	65	426.78	5.00
PM	(o)	C6Cn.3n	23.30	50R-1,	0			469.00	9.00
PM	(y)	C7An	24.76	63R-3,	85	63R-3,	120	597.12	0.17
PM	(o)	C7An	24.98	64R-1,	130	64R-1,	135	604.33	0.02
PM	(o)	C8n.1n	25.26	68R-2,	20	68R-2,	75	643.38	0.27
PM	(y)	C8n.2n	25.30	69R-2,	20	69R-2,	25	652.58	0.02
PM	(o)	C8n.2n	25.99	71R-6,	115	72R-1,	10	678.98	0.92
PM	(y)	C9n	26.42	73R-4,	90	75R-1,	15	701.66	7.09
PM	(o)	C9n	27.44	76R-6,	35	76R-6,	40	725.09	0.02
PM	(o)	C11n.2n	29.97	82R-6,	35	82R-6,	40	782.68	0.03
PM	(y)	C13n	33.16	93R-1,117		93R-2,	28	878.00	0.23

993

Table 3

In situ taxa
Adnatosphaeridium? sp.
Ataxodinium choane
Batiacasphaera compta
Batiacasphaera spp. (pars.)
Batiacasphaera hirsuta
Batiacasphaera micropapillata
Batiacasphaera minuta
Batiacasphaera sphaerica
Batiacasphaera sp. A
Batiacasphaera sp. B
Batiacasphaera sp. C
Batiacasphaera sp. D
Brigantedinium simplex
Brigantedinium pynei
Brigantedinium sp. A
Brigantedinium sp. B
Brigantedinium sp. C
Brigantedinium sp. D
Cerebrocysta WR small
Cerebrocysta delicata
Cerebrocysta sp. A
Cleistosphaeridium sp. B
Cleistosphaeridium sp.A
Cordosphaeridium minutum
Corrudinium labradori
Corrudinium sp. A
Cryodinium? sp.
Distatodinium spp.
Edwardsiella sexispinosa
Elytrocysta sp. A
Elytrocysta brevis
Gelatia inflata
Habibacysta? spp.
Homotryblium spp.
Hystrichokolpoma bullatum
Huystrichosphaeropsis obscura
Impagidinium spp. (pars)
Impagidinium aculeatum
Impagidinium cantabrigiense
Impagidinium elegans
Impagidinium elongatum
Impagidinium pacificum
Impagidinium pallidum
Impagidinium paradoxum
Impagidinium patulum
Impagidinium plicatum
Impagidinium velorum
Impagidinium victorianum
Impagidinium sp. A
Impagidinium sphaericum
Invertocysta tabulata
Islandinium spp.
Lejeunecysta attenuata
Lejeunecysta adeliense
Lejeunecysta fallax
Lejeunecysta cowei
Lejeunecysta acuminata
Lejeunecysta rotunda
Lejeunecysta katatonos
Malvinia escutiana
Nematosphaeropsis labyrinthus
Oligokolpoma galeotti
Operculodinium tiara
Operculodinium sp. A
Operculodinium piaseckii
Operculodinium janduchenei
Operculodinium cf *eirikianum*
Operculodinium eirikianum
Paleocystodinium golzowense
Paucisphaeridium spp.
Phthanoperidinium amoenum
Pyxidinopsis spp. (pars)
Pyxidinopsis sp. A
Pyxidinopsis sp. B
Pyxidinopsis sp. C
Pyxidinopsis sp. D
Pyxidinopsis vesciculata
Pyxidinopsis tuberculata
Pyxidinopsis reticulata
Pyxidinopsis fairhavensis
Reticulatosphaera actinocoronata
Selenopemphix antarctica
Selenopemphix nephroides
Selenopemphix dioneacysta
Selenopemphix sp. A
Selenopemphix undulata
Selenopemphix brinkhuisi
Spiniferites sp. B
Spiniferites sp. A
Spiniferites sp. C
Stoveracysta ornata
Stoveracysta kakanuiensis
?*Svalbardella* spp.
Tectatodinium spp.
Unipontedinium aquaeductus
Protoperidinioid indet
Protoperidinium sp. B
Protoperidinium sp. A
Protoperidinium sp. C
Protoperidinium sp. D

Reworked taxa
Achilleodinium biformoides
Achomosphaera alcicornu
Aiora fenestrata
Aireiana verrucosa
Adnatosphaeridium spp.
Alisocysta circumtabulata
Alterbidinium distinctum
Apectodinium spp.
Arachnodinium antarcticum
Areoligera spp. (pars)
Areoligera semicirculata
Cerebrocysta bartonensis
Charlesdowniea clathrata
Charlesdowniea edwardsii
Cooksonidinium capricornum
Cordosphaeridium fibrospinosum
Cordosphaeridium furniculatum
Corrudinium incompositum
Corrudinium regulare
Cribroperidinium spp.
Damassadinium crassimuratum
Dapsilidinium spp.
Deflandrea sp. A sensu Brinkhuis et al., 2003
Deflandrea antarctica
Deflandrea cygniformis
Diphyes colligerum
Deflandrea spp. Indet
Eisenackia circumtabulata
Enneadocysta diktyostila
Enneadocysta multicornuta
Eocladopyxis tesselata
Fibrocysta axialis
Glaphyrocysta intricta
Glaphyrocysta pastielsii
Heteraulacacysta leptalea
Histiocysta palla
Hystrichokolpoma pusilla
Hystrichokolpoma rigaudiae
Hystrichokolpoma truncatum
Hystrichosphaeridium truswelliae
Hystrichosphaeridium tubiferum
Impagidinium maculatum
Impagidinium waipawense
Kenleyia spp.
Manumiella druggii
Melitasphaeridium pseudorecurvatum
Membranophoridium perforatum
Octodinium askiniae
Odontochitina spp.
Operculodinium spp.
Phthanoperidinium antarcticum
Phthanoperidinium echinatum
Polysphaeridium spp.
Rhombodinium sp.
Schematophora speciosa
Schematophora obscura
Senegalinium spp.
Spinidinium luciae
Spinidinium macmurdoense
Spinidinium schellenbergii
Spiniferites ramosus CPX
Thalassiphora pelagica
Turbiosphaera filosa
Turbiosphaera sagena
Vozzhennikovia apertura/ S.schellenbergii group
Vozzhennikovia netrona
?*Vozzhenikovia* LARGE
Wetzeliella articulata

994